AD-A146 718 RESOLVE (RESEARCH ON OPERATIONS-LIMITING VISUAL EXTINCTION) MONITORING PR..(U) LOCKHEED ENGINEERING AND MANAGEMENT SERVICES CO INC LAS VEGAS.. 1/1

UNCLASSIFIED J TRIJONIS ET AL. SEP 84 NWC-TR-6567 F/G 20/6 NL

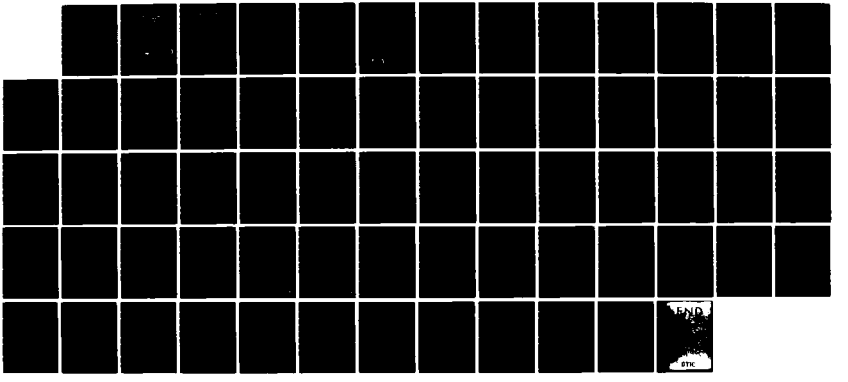

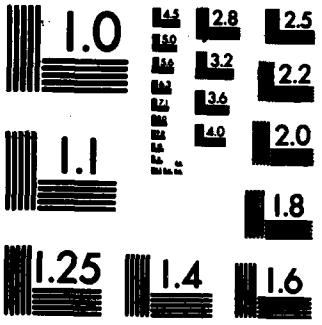
1.0
1.1
1.25
1.4
1.6
1.8
2.0
2.2
2.5
2.8
3.2
3.6
4.0

(12)

NWC TP 6567

RESOLVE Monitoring Program Plan Evaluation Using Historical Data and Error Analysis

by
John Trijonis
Santa Fe Research Corp.
and
John Watson
Alan Waggoner
Raymond Weiss
Desert Research Institute
for the
Public Works Department

SEPTEMBER 1984

NAVAL WEAPONS CENTER
CHINA LAKE, CA 93555-6001

Naval Weapons Center

AN ACTIVITY OF THE NAVAL MATERIAL COMMAND

FOREWORD

The atmospheric visibility study documented in this report was performed during 1984 for the Department of Defense and the EPA Environmental Monitoring Systems Laboratory under contract EPA68-03-3050 to the Santa Fe Research Corp. by Lockheed–EMSCO.

Because of the continuing nature of the research, refinements and modifications may later be made in this study.

Approved by
H. H. HARRELL
Capt., CEC, USN
Public Works Officer
12 September 1984

Under authority of
K. A. DICKERSON
Capt., USN
Commander

Released for publication by
B. W. HAYS
Technical Director

NWC Technical Publication 6567

Published by ..... Technical Information Department
Collation ..... Cover, 33 leaves
First printing ..... 170 copies

UNCLASSIFIED

SECURITY CLASSIFICATION OF THIS PAGE (When Data Entered)

REPORT DOCUMENTATION PAGE	READ INSTRUCTIONS BEFORE COMPLETING FORM
1. REPORT NUMBER NWC TP 6567	2. GOVT ACCESSION NO. AD-A146 718 / 3. RECIPIENT'S CATALOG NUMBER
4. TITLE (and Subtitle) RESOLVE MONITORING PROGRAM PLAN EVALUATION USING HISTORICAL DATA AND ERROR ANALYSIS	5. TYPE OF REPORT & PERIOD COVERED 6. PERFORMING ORG. REPORT NUMBER
7. AUTHOR(s) John Trijonis, Santa Fe Research Corp. John Watson Alan Waggoner Raymond Weiss, Desert Research Institute	8. CONTRACT OR GRANT NUMBER(s) EPA68-03-3050
9. PERFORMING ORGANIZATION NAME AND ADDRESS Santa Fe Research Corp. 11200 Bloomington Ferry Rd. Bloomington, MN 55438	10. PROGRAM ELEMENT, PROJECT, TASK AREA & WORK UNIT NUMBERS
11. CONTROLLING OFFICE NAME AND ADDRESS Naval Weapons Center China Lake, CA 93555-6001	12. REPORT DATE September 1984 13. NUMBER OF PAGES 64
14. MONITORING AGENCY NAME & ADDRESS(if different from Controlling Office)	15. SECURITY CLASS. (of this report) UNCLASSIFIED 15a. DECLASSIFICATION/DOWNGRADING SCHEDULE

16. DISTRIBUTION STATEMENT (of this Report)

Approved for public release; distribution is unlimited.

17. DISTRIBUTION STATEMENT (of the abstract entered in Block 20, if different from Report)

18. SUPPLEMENTARY NOTES

19. KEY WORDS (Continue on reverse side if necessary and identify by block number)

Atmospheric visibility	RESOLVE
Nephelometry	Visibility, atmospheric
California desert	Visual extinction

20. ABSTRACT (Continue on reverse side if necessary and identify by block number)

See back of form.

DD FORM 1 JAN 73 1473 EDITION OF 1 NOV 65 IS OBSOLETE

S/N 0102-LF-014-6601

UNCLASSIFIED

SECURITY CLASSIFICATION OF THIS PAGE (When Data Entered)

(U) *RESOLVE Monitoring Program Plan Evaluation Using Historical Data and Error Analysis*, by John Trijonis, Santa Fe Research Corp.; and John Watson, Alan Waggoner, and Raymond Weiss, Desert Research Institute. China Lake, Calif., Naval Weapons Center, September 1984. 64 pp. (NWC TP 6567, publication UNCLASSIFIED.)

(U) Three specific issues are analyzed in a major study (RESOLVE: Research on Operations-Limiting Visual Extinction) of atmospheric visibility in the California desert. (1) The issue of the contribution of NO_2 to light extinction is investigated using aircraft measurements taken as part of the California Air Resources Board (CARB) Los Angeles/desert transport study, routine historical data for NO_2 and visual range, and a small amount of data acquired with high-resolution research-type NO_2 monitoring. (2) An assessment is made of the adequacy of 24-hour particle samples as compared to 8-hour particle samples with respect to characterizing visibility during daylight hours. (3) An investigation is made into the propagation of measurement errors through to the final modeling results for extinction budgets and particle source apportionments for the RESOLVE program.

CONTENTS

1.0 INTRODUCTION

The Department of Defense and the Environmental Protection Agency (EPA) Environmental Monitoring Systems Laboratory are conducting a major study of atmospheric visibility in the California desert. The name of this study is RESOLVE–Research on Operations-Limiting Visual Extinction. The supporting contractor for DOD and EPA is Lockheed-EMSCO, Las Vegas, Nev., who is responsible for much of the field monitoring program.

The agencies and organizations conducting RESOLVE have been establishing an extensive and sophisticated monitoring program to provide the basic data for the study. It became apparent, however, that before finalizing the monitoring program, there was a need to settle certain issues through literature surveys, analyses of historical data sets, and error studies. Three specific issues that needed to be addressed were as follows:

1. Determine if the contribution of NO_2 to light extinction in the study area is low enough so that NO_2 need not be measured on a routine basis.

2. Assess the adequacy of 24-hour particle samples as compared to 8-hour particle samples with respect to characterizing visibility during daylight hours.

3. Investigate the propagation of potential RESOLVE measurement errors through to the final modeling results for extinction budgets and particle source apportionments.

The analyses of these three issues are presented in Sections 2 through 4, respectively, of this report.

1.1 ORGANIZATION

The work reported herein was performed under a contract to Santa Fe Research Corp. by Lockheed-EMSCO. Santa Fe Research Corp. had the primary research responsibility for the analysis of NO_2 extinction contributions (Section 2) and the study of 8-hour versus 24-hour particle sampling (Section 3). The error propagation analysis (Section 4) was conducted via a subcontract to Desert Research Institute. Two consultants, Alan Waggoner and Raymond Weiss, provided the data for Section 3 as well as general assistance on the other aspects of the project.

1.2 SUMMARY OF CONCLUSIONS AND RECOMMENDATIONS

The issue of the contribution of NO_2 to extinction is investigated in this report using three data bases: measurements made from aircraft, taken as part of the California Air Resources Board (CARB) Los Angeles/desert transport study, routine historical data for NO_2 and visual range, and a small amount of data acquired with high-resolution research-type NO_2 monitoring. All three data bases suggest that, on the average, fractional NO_2 contributions to total extinction in the California desert are generally less than 5%, maybe substantially less than 5%. Accordingly, it

does not appear necessary to monitor NO_2 on a routine basis as part of RESOLVE. Nevertheless, to become more certain regarding the role of NO_2, two further steps are recommended. First, when hourly NO_2 measurements are compiled as part of the data base for the California Desert Air Working Group (CDAWG), the measurements should be examined to study NO_2 contributions under worst-case conditions. Second, the RESOLVE "special intensive studies" should include some NO_2 monitoring with high-sensitivity instruments at the Naval Weapons Center (NWC), China Lake, and Edwards AFB, Calif.

A study of historical nephelometry data for the California desert reveals that significant diurnal variations exist in fine particle concentrations. These variations do not necessarily imply, however, that source mixtures for fine particles tend to vary significantly over the day. In fact, a high correlation between 8-hour (0800 to 1600 PST) and 24-hour nephelometer averages indicates that daytime and 24-hour particulate concentrations are not uncoupled. Furthermore, an examination of available particulate composition data with diurnal resolution suggests that daytime and nighttime particulate source mixtures are the same in an average sense. Because of these findings, because of procedural difficulties and extra expenses associated with short-term particle sampling, and because of some interest in nighttime as well as daytime visibility for DOD operations, it seems prudent to begin the routine RESOLVE program with 24-hour particle sampling. It is recommended, however, that further study of this issue be conducted. The drum sampler data from RESOLVE should be analyzed regarding daytime/nighttime differences in particle contributions from sulfates and soil. Moreover, as part of the special intensive studies for RESOLVE, the particle samplers should be run on a daytime and nighttime basis.

Least squares solutions to the mass balance and scattering budget receptor models that provide uncertainty estimates for model results are derived herein. Applications of these models to randomized data derived from known source contributions and known scattering efficiencies show that the calculated uncertainties are good estimates of the real uncertainties, even when the measurement uncertainty levels are as high as 30%. To characterize and minimize the uncertainty of the interpretive analysis results, the RESOLVE program should document and minimize the measurement uncertainties and maximize the number of sampling cases.

2.0 CONTRIBUTION OF NO_2 TO LIGHT EXTINCTION LEVELS IN THE CALIFORNIA DESERT

Total light extinction consists of a simple sum of four terms: light scattering by particles (usually dominated by sulfates and other fine aerosols), light absorption by particles (dominated by elemental carbon), light scattering by air molecules (natural Rayleigh scatter), and light absorption by gases (basically all from NO_2). A preliminary working hypothesis of the RESOLVE study is that light absorption by NO_2 is an insignificant component of regional extinction in the California desert. This hypothesis is based on the following argument. In the Los Angeles Basin and San Joaquin Valley, the major source areas upwind of the California desert, the average contribution of NO_2 to total extinction is about 8%.* We would expect, however, relatively lesser NO_2 contribution in the desert. One basic reason is that transported particles have slow

* A table of published results regarding NO_2 extinction contributions in the source areas is as follows:

Los Angeles Basin - - -	8%	2 sites (Reference 1)
	10%	1 site (Reference 2)
	5-13%	9 sites (Reference 3)
San Joaquin Valley - - -	7-8%	3 sites (Reference 3)

removal rates, while transported NO_2 is continuously depleted by oxidation to nitric acid, conversion to particles, and deposition to surfaces. Furthermore, as the particle and NO_2 pollution is diluted during transport, the background Rayleigh scatter term becomes relatively more significant, reducing the overall percentage contribution from both particles and NO_2.

Because of the above hypothesis, the acquisition of NO_2 data on a routine basis is not currently planned as part of RESOLVE. It is very important, nevertheless, to check the assumption regarding NO_2 levels in the study area. The purpose of this chapter is to estimate NO_2 contributions to extinction in the California desert by analyzing currently available data.

2.1 CARB LOS ANGELES/DESERT TRANSPORT STUDY

No data base exists that can provide a definitive answer regarding NO_2 extinction contributions in non-urban parts of the California desert. The best data available come from an aircraft survey by Meteorology Research, Inc. (MRI), Altadena, Calif., conducted as part of the Los Angeles/desert transport study sponsored by CARB (Reference 4). The MRI survey may, however, overestimate typical NO_2 contributions in the desert because the survey was designed to study transport phenomena from Los Angeles rather than remote desert conditions.

Table 2-1 summarizes average particle scattering (b_{sp}) and average NO_2 concentrations for desert flight paths during the survey. The percent contribution of NO_2 extinction (b_{NO_2} or b_{ag}) to total extinction, $b_{ag}/(b_{sg} + b_{sp} + b_{ag} + b_{ap})$, is calculated from these data as follows:

b_{ag} = NO_2 absorption at 550 nm (nanometers) = $0.033 \cdot [NO_2]$, with units of b_{ag} in $10^{-4}m^{-1}$ and units of $[NO_2]$ in pphm (parts per hundred million) as listed in Table 2-1.
b_{sg} = Rayleigh scatter = 0.12 $10^{-4}m^{-1}$.
b_{sp} = particle scattering = as listed in Table 2-1.
b_{ap} = particle absorption = assumed to be 10% of b_{sp}.

TABLE 2-1. Aircraft NO_2 and BSCAT Data by MRI, July – August 1981.

Date	Time	Site	b_{sp} ($10^{-4}m^{-1}$)	NO_2, pphm	NO_2 contribution to total estimated extinction, %[a]
7/09	1622	Cajon Pass	0.46	1.0	5
7/09	1655	Cajon Pass	0.41	0.8	4
7/09	1720	Cajon Pass	0.66	1.2	4
7/14	1750	Palmdale	0.57	1.0	4
7/14	1908	Victorville	0.87	1.8	5
7/15	0913	Palmdale	0.29	0.3	2
7/15	1008	Barstow	0.38	0.7	4
7/18	1800	Palmdale	1.13	1.5	4
7/27	1645	Victorville	0.59	0.9	4
7/30	1530	Victorville	0.33	0.3	2

[a] NO_2 fractional contribution = $\frac{b_{ag}}{b_{sg} + b_{sp} + b_{ag} + b_{ap}}$, where s = scattering, a = absorption, g = gas, and p = particles.

Table 2-1 shows that the contribution of NO_2 to total extinction during the MRI surveys averaged 2 to 5%. As noted above, these contributions may be higher than those typically found in remote parts of the desert not under the direct influence of transport from Los Angeles.

2.2 ROUTINE LONG-TERM DATA BASES

Another way of estimating the fraction of extinction caused by NO_2 in the California desert is to analyze the historical data bases for routine NO_2 monitoring and airport visibility. Trijonis (Reference 5) has published an isopleth map of median airport visibility levels throughout California, including the desert. Median (1300) visual ranges, taken from that map, can be converted into estimates of total extinction using a Koschmeider constant of 3.0 (b = 3.0/V), the appropriate constant for airport visibility data (Reference 3).

Long-term continuous NO_2 data are available from CARB and, to a lesser extent, from Southern California Edison (SCE) Co. Values of NO_2 at 1300 were compiled from the CARB data so that they would correspond to the 1300 airport visibility data (only annual means of all hours were readily available for the SCE NO_2 data). The CARB NO_2 data are rather coarse for desert conditions in the sense that values are reported only to the nearest pphm. In determining median NO_2 from the data, cumulative frequency distributions were calculated assuming 0 pphm recordings meant concentrations below 0.5 pphm, 1 pphm recordings meant concentrations between 0.5 pphm and 1.5 pphm, etc. These frequency distribitions appeared generally well-behaved when plotted on log-normal paper; the medians were estimated by interpolations of lines fit to the log-normal plots. The median NO_2 concentrations were translated into NO_2 extinction levels using the formula discussed in the previous section.

The results of the analysis are presented in Table 2-2. These results, although more variable than those in Table 2-1, are consistent with Table 2-1 in suggesting that the fraction of extinction caused by NO_2 in the desert averages about 4%. It should be noted that we strongly suspect that these findings represent *overestimates* of actual NO_2 contribution to extinction in *non-urban* areas of the desert. The reason is that most of the sites in Table 2-2 involve a comparison of NO_2 in towns or small urbanized areas with a long path measurement of visual range extending over rural areas. The NO_2 concentrations in the small urbanized areas are probably greater than the average NO_2 concentrations over the site path. Finally, it should be noted that the variations from site to site in Table 2-2 do not seem readily explainable and may be due to the inadequacies of this somewhat crude analysis.

We had also hoped to analyze these data sets for fractional NO_2 contributions to extinction under individual "worst-case" conditions. This analysis would require an airport located near a *non-urban* desert monitoring site. It turned out that no such pairing of sites existed. In the future, we hope to obtain b_{sp} and NO_2 data from one or two remote SCE sites that can be studied regarding worst-case episodes. Such data will become available when a data base compilation study now being conducted by CDAWG is completed.

2.3 HIGH-SENSITIVITY NO_2 MONITORS

The above analyses are based on data from "off-the-shelf" NO_2 monitors. Because NO_2 concentrations are very low in the desert, the observations generally occur near the detection thresholds of the instruments. We have found one NO_2 data set for the Mojave Desert taken with a

high-sensitivity, low-zero uncertainty NO_2 monitor (Reference 6). For these measurements, taken during September 1983, NO_2 concentrations were always below 1 pphm, and generally below 0.5 pphm. Assuming a typical total extinction level of 0.4 $10^{-4}m^{-1}$, NO_2 concentrations of 0.5 pphm would represent 4% of total extinction.

TABLE 2-2. Median Midday NO_2 and Visibility Data for Desert Sites.

City (population)	Median (1300) NO_2, pphm	Median (1300) annual visual range, mi.	NO_2 contribution to extinction, %
CARB DATA			
Victorville (11,000)	0.6[a]	33[b]	4[c]
Barstow (17,000)	0.7	36	5
Lancaster (35,000)	0.5	30	3
Indio (15,000)	0.7	30	4
Palm Springs (21,000)	1.0	24	4
Trona (1,500)	0.6	65	7
Palo Verde (0?)	0.7	60	8
SCE DATA			
Coolwater (2,000?)	1.1[d]	36	7
Lucerne Valley (0?)	0.3	35	½

[a] Provided by CARB.

[b] (Reference 5)

[c] Using a Koschmeider constant of 3.0 (5% contrast level) to convert airport median visibility into extinctions, and using the NO_2 extinction coefficient given in the text.

[d] Provided by SCE.

2.4 CONCLUSIONS

All of the analyses conducted in this chapter suggest that fractional NO_2 contributions to total extinction in the California desert are generally less than 5%, maybe significantly less than 5%, given that the techniques tended to yield overestimates. Accordingly, it does not appear necessary to monitor NO_2 on a routine basis as part of RESOLVE. Nevertheless, to become more certain regarding the role of NO_2, two further steps are recommended. First, when the CDAWG data base becomes available, some of the SCE data for NO_2 and b_{sp} should be examined to study NO_2 contributions under episode conditions. Second, the RESOLVE special intensive studies should include some NO_2 monitoring with *high-sensitivity* instruments at NWC and Edwards AFB.

3.0 ADEQUACY OF 24-HOUR PARTICLE SAMPLING SCHEDULE

With respect to the current RESOLVE monitoring plan, there is a question as to whether the 24-hour fine particle samples are adequate to address *daytime* visibility problems. Specifically, concern exists whether daytime particle source mixtures might differ significantly from 24-hour average source mixtures. The purpose of this section is to evaluate the adequacy of 24-hour particle samples as compared to 8-hour daytime particle samples. This issue will be addressed by conducting three types of analyses: assessing the importance of and causes for diurnal variations in existing nephelometry data (Section 3.1), examining the predictability of 8-hour average b_{sp} (fine particle scattering) from 24-hour average b_{sp} (Section 3.2), and studying daytime/nighttime particulate composition data published in Ouimette's Ph.D. thesis (Section 3.3) (Reference 7).

Each of the three planned analyses has significant limitations. The first two are based on a large volume (several years) of nephelometry data, but they do not explicitly address the problem of diurnal variations in particulate chemical composition (i.e., particulate source mixture). The third analysis examines actual chemical composition data, but it is based on only a few days of sampling in one season. Combining all three analyses, however, should provide fairly sound recommendations for the RESOLVE sampling program (Section 3.4).

3.1 DIURNAL VARIATIONS IN NEPHELOMETRY DATA

One way of shedding light on the issue of day/night variations in fine particle source mixtures is to examine the diurnal patterns in the historical nephelometry (b_{sp}, particle scattering) data base for the study area. Are the diurnal patterns in b_{sp} (i.e., fine particle concentrations) important or insignificant? Are the diurnal patterns likely associated with significant shifts in particle sources?

Figures 3-1 through 3-5 plot annual average diurnal patterns for five DOD nephelometer sites in the California desert. In order to avoid seasonal biases in the annual plots, the analysis is limited only to years for which *complete* data were available at the time of this study. The analysis is further restricted to days providing at least 18 hours of valid data (nearly all days meet this restriction). Diurnal patterns for each site on a monthly basis are presented in the appendix to this report.

Each appendix figure contains two lines, representing two ways of calculating the diurnal patterns. The solid line simply represents the annual average value for each hour; it is measured by the ordinate axis labeled "b_{sp}." The dashed line represents an average, over the year, of the fractional change away from the mean value each day. The latter index, measured on the left ordinate axis labeled "$(b_{sp} - b_{ave})/b_{ave}$," is an indication that weights days of low concentrations on an equal basis with days of high concentrations in calculating the diurnal patterns.

With the exception of the Death Valley results,* Figures 3-1 through 3-5 reveal strong diurnal patterns in fine particle concentrations (i.e., b_{sp}), with a distinct minimum in the early

* There are several alternate hypotheses regarding the lack of a significant diurnal pattern at Death Valley. One conjecture is that transported pollution may be homogenized on a very large scale by the time it reaches the distant site at Death Valley, so that diurnal dispersion variations do not necessarily produce diurnal changes in concentrations.

afternoon. One possible explanation is that local source emissions (e.g., from woodburning or spaceheating in the winter) might accumulate during the evening to produce the observed diurnal pattern. This might imply a distinct day/night difference in particle source composition. However, another possible explanation is that fine particle concentration elevation in the late afternoon and evening is due to transport from upwind air basins and that the daytime minimum simply reflects the dilution of this air mass with increased mixing height during the afternoon. This latter explanation, which seems supported by the fact that the diurnal pattern is greatest during the *summer* (see Appendix), would be consistent with an equivalent source mixture during day and night. In any case, the strong diurnal patterns do suggest that the issue of 24-hour versus 8-hour sampling must be given careful scrutiny.

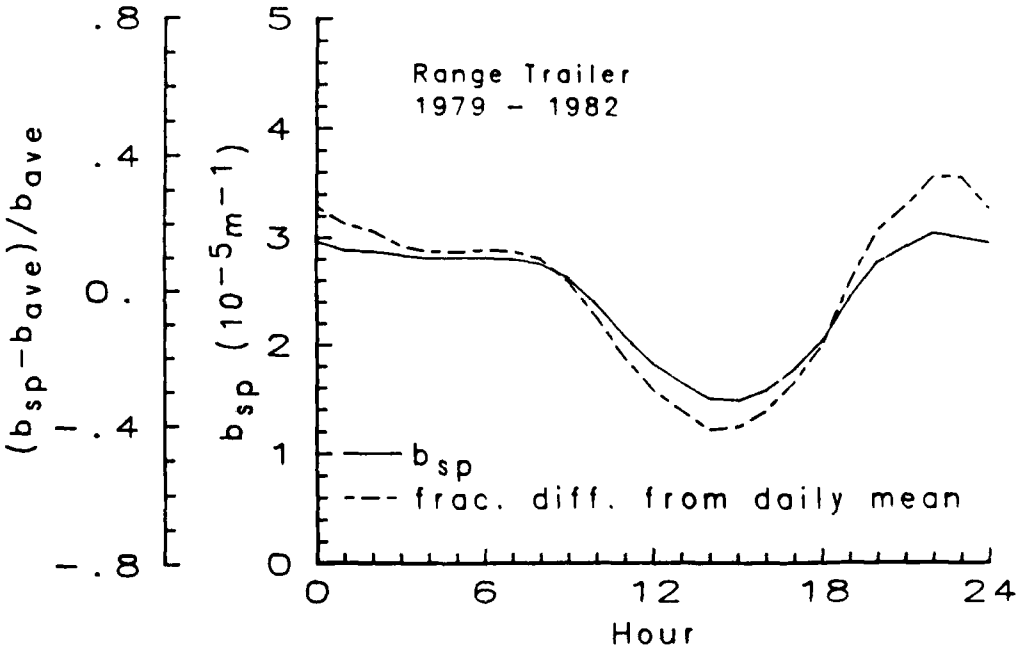

FIGURE 3-1. Diurnal Pattern of Particle Scattering at China Lake Range Trailer.

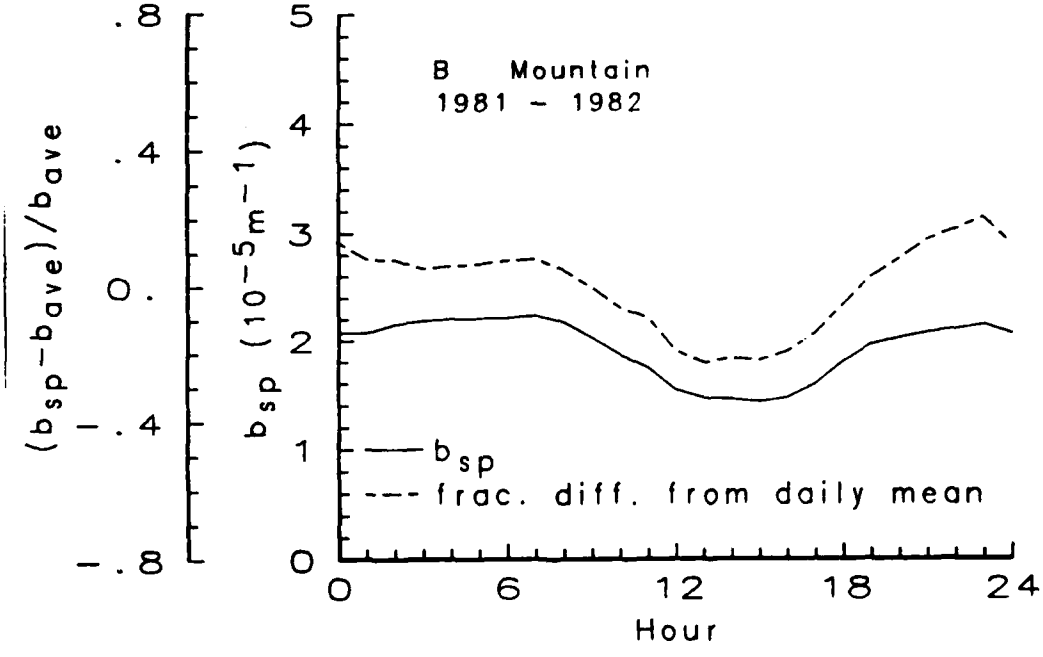

FIGURE 3-2. Diurnal Pattern of Particle Scattering at China Lake B Mountain.

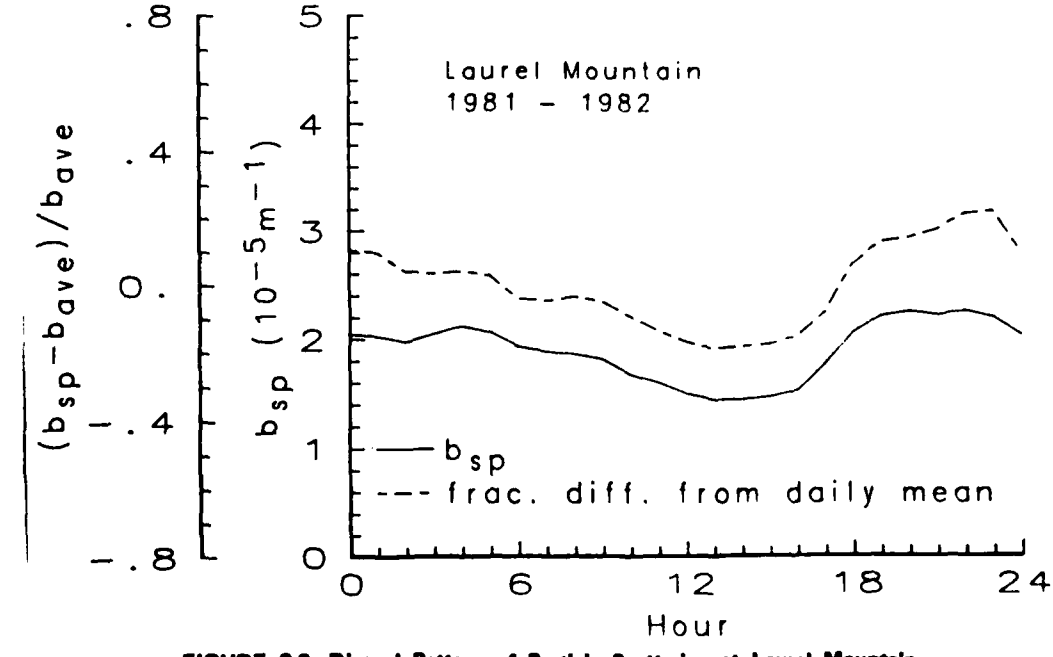

FIGURE 3-3. Diurnal Pattern of Particle Scattering at Laurel Mountain Near China Lake.

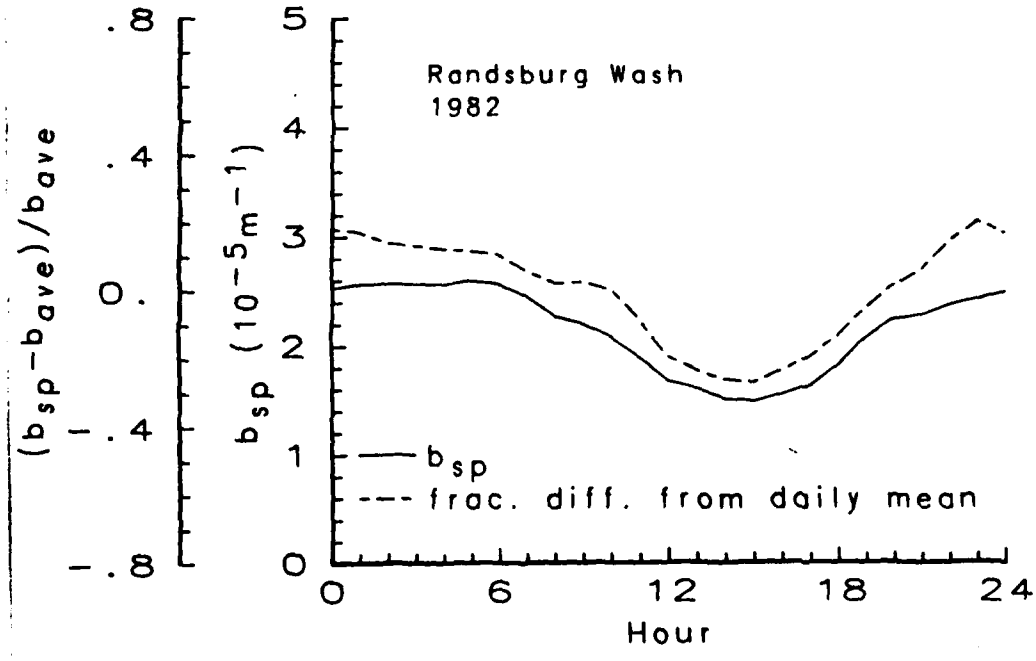

FIGURE 3-4. Diurnal Pattern of Particle Scattering at Randsburg Wash.

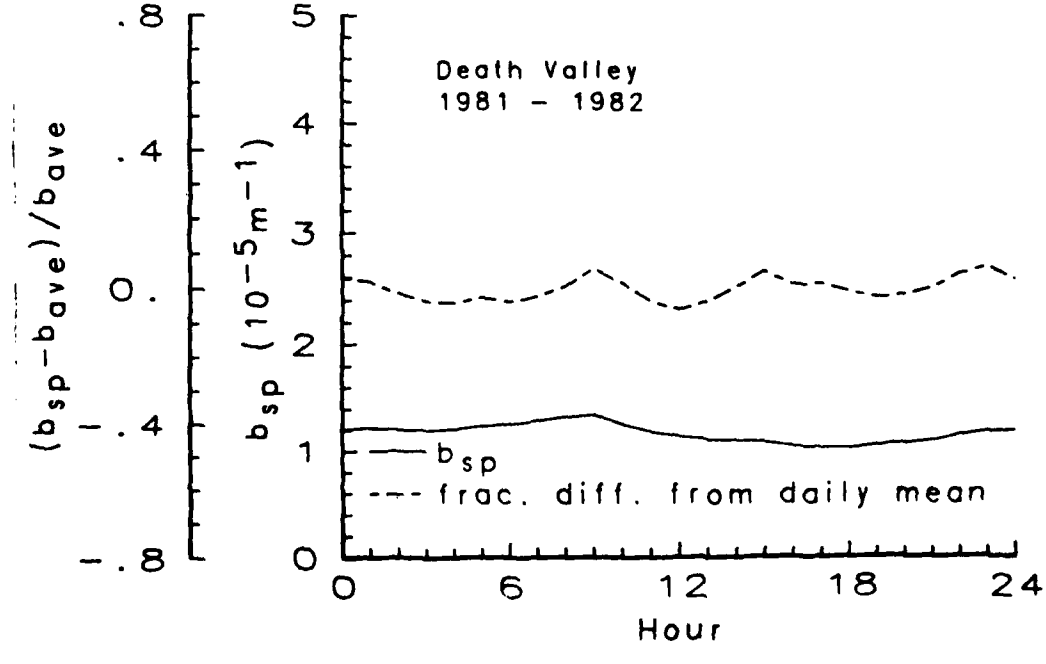

FIGURE 3-5. Diurnal Pattern of Particle Scattering at Death Valley.

3.2 CORRELATION OF 8-HOUR VERSUS 24-HOUR NEPHELOMETRY DATA

For further analysis, the nephelometry data at the five California desert sites were organized into three 8-hour averages as well as a single 24-hour average each day. The main purpose was to correlate the 24-hour average with the daytime (0800-1600) 8-hour average (see lower righthand corners of Figures 3-6 through 3-10). In addition, we used these data sets to plot the diurnal patterns in terms of 8-hour averages (upper lefthand corners of Figures 3-6 through 3-10), the 24-hour average seasonal patterns by quarters of the year (upper righthand corners of the figures), and the 8-hour diurnal patterns by quarters (lower lefthand corners of the figures).

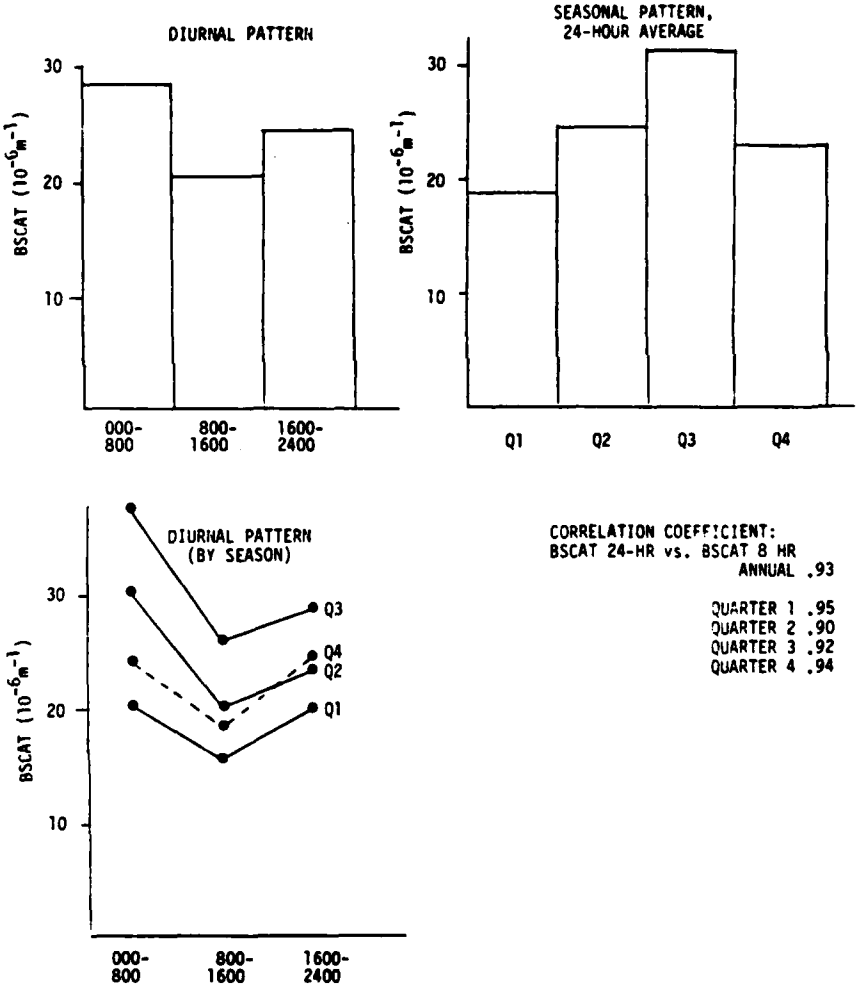

FIGURE 3-6. Diurnal Patterns, Seasonal Variations, and Correlations for 8-Hour and 24-Hour Particle Scattering at China Lake Range Trailer.

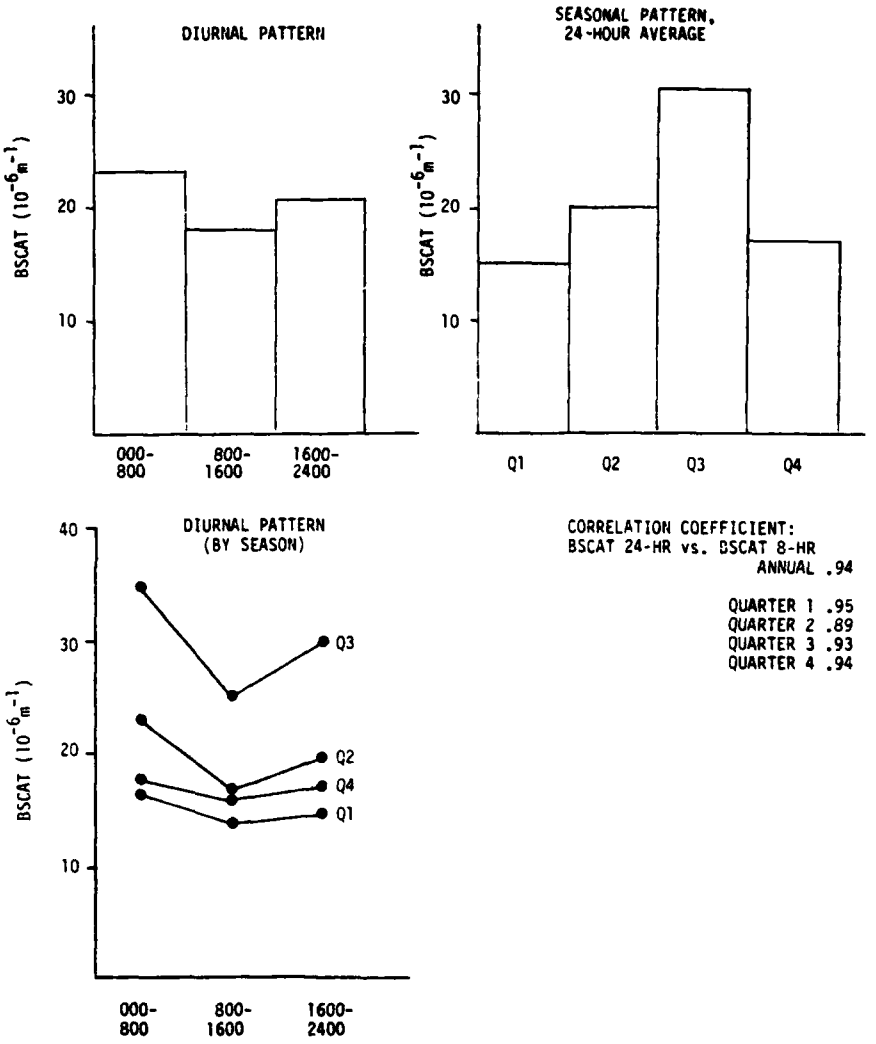

FIGURE 3-7. Diurnal Patterns, Seasonal Variations, and Correlations for 8-Hour and 24-Hour Particle Scattering at China Lake B Mountain.

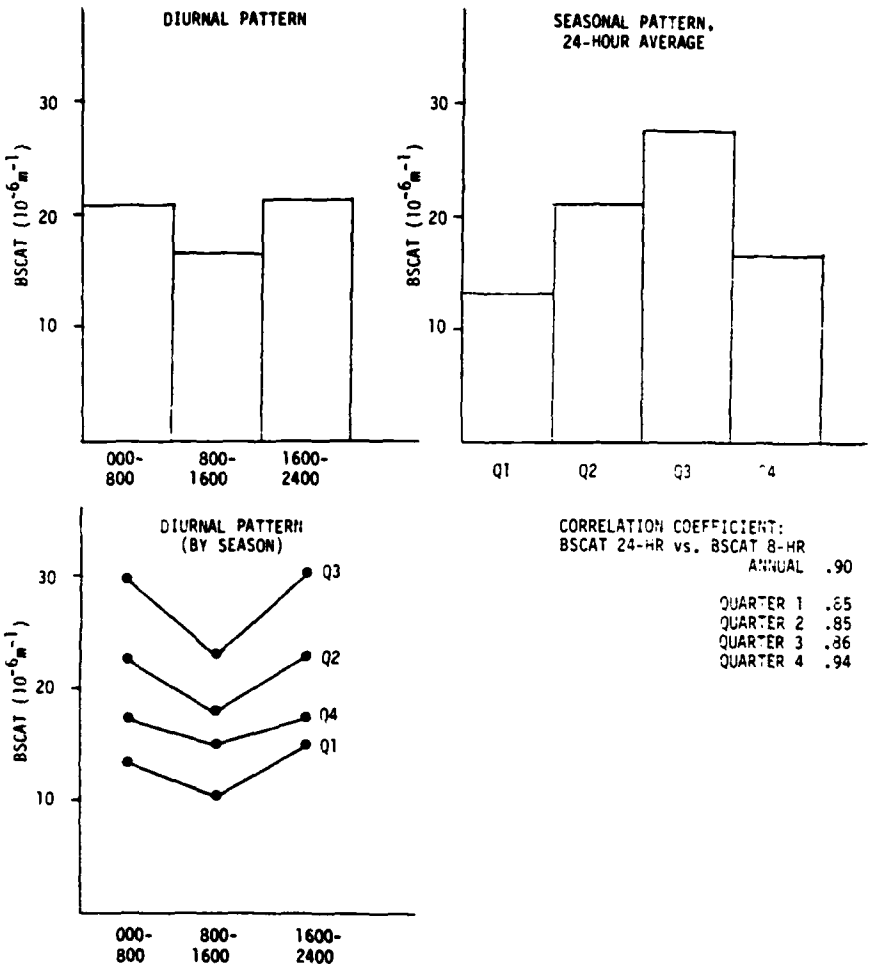

FIGURE 3-8. Diurnal Patterns, Seasonal Variations, and Correlations for 8-Hour and 24-Hour Particle Scattering at Laurel Mountain Near China Lake.

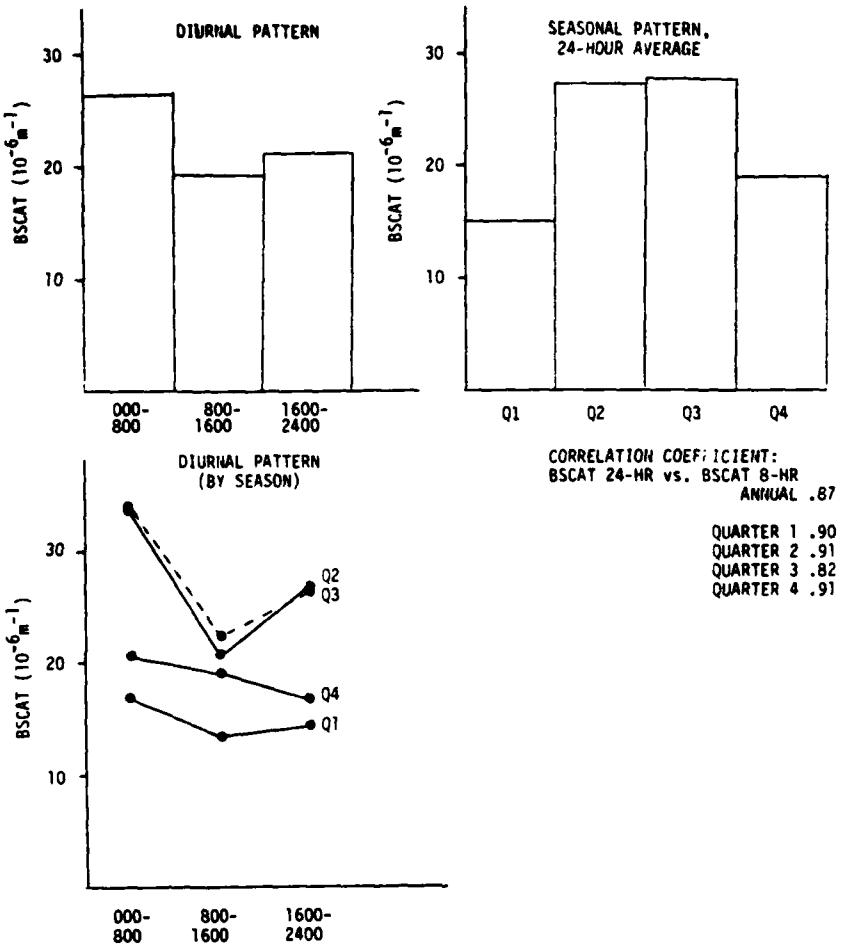

FIGURE 3-9. Diurnal Patterns, Seasonal Variations, and Correlations for 8-Hour and 24-Hour Particle Scattering at Randsburg Wash.

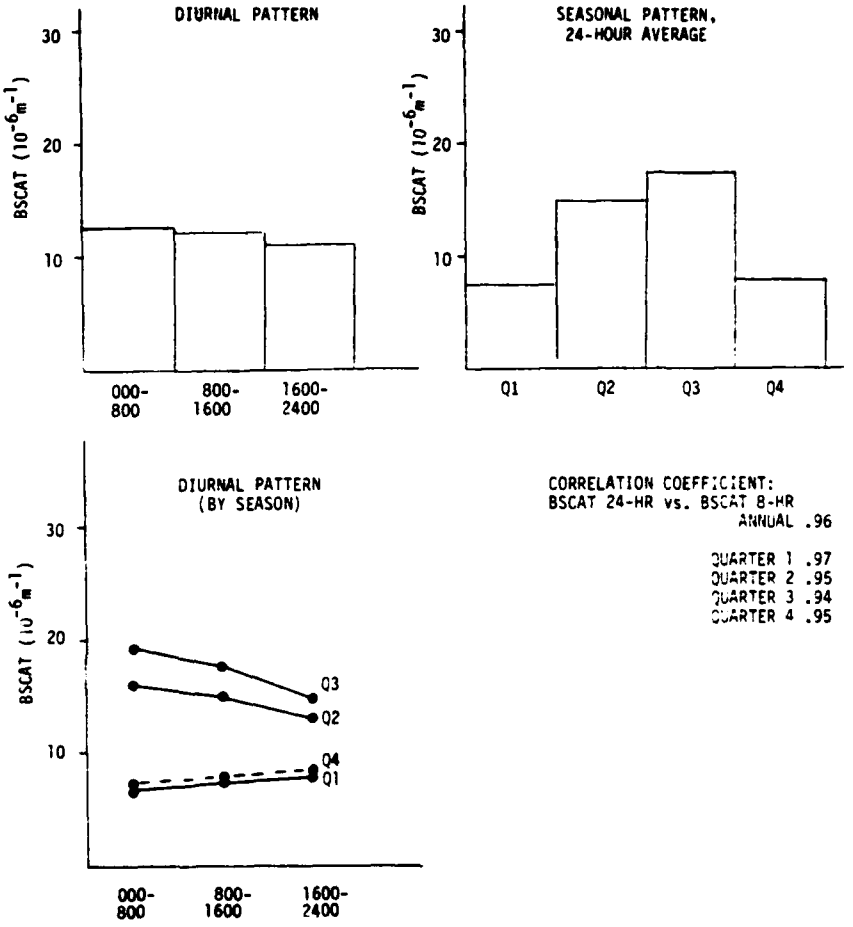

FIGURE 3-10. Diurnal Patterns, Seasonal Variations, and Correlations for 8-Hour and 24-Hour Particle Scattering at Death Valley.

Table 3-1 summarizes the correlations between the daily 24-hour average and the daytime 8-hour averages for each of the five sites. The correlations are presented for the entire data set (annual) as well as for the data disaggregated by seasonal quarter. Table 3-1 shows that the correlations are uniformly high, generally between about 0.90 and 0.95. This means that 24-hour average b_{sp} can serve as a fairly precise predictor of 8-hour daytime b_{sp}. It further implies that the daytime and 24-hour variations in fine particle concentrations are certainly *not uncoupled*. This is the first piece of evidence hinting that 24-hour particle sampling may be adequate for characterizing the 8-hour daytime period. Specifically, even though the 8-hour daytime averages are generally lower than the 24-hour averages (as demonstrated by the diurnal patterns), the 8-hour averages appear to be consistently related to the 24-hour averages (as indicated by the high correlations). This coupling further suggests, but does not prove, similar particle source compositions for the 8-hour and 24-hour averages.

TABLE 3-1. Correlation Coefficients Between Daily 24-Hour and Daytime 8-Hour Nephelometry Averages.

Area	Annual	Quarterly			
		1	2	3	4
China Lake Range Trailer	0.93	0.95	0.90	0.92	0.94
B Mountain	0.94	0.95	0.89	0.93	0.94
Laurel Mountain	0.90	0.85	0.85	0.86	0.94
Randsburg Wash	0.87	0.90	0.91	0.82	0.91
Death Valley	0.96	0.97	0.95	0.94	0.95

3.3 DAY/NIGHT PARTICULATE COMPOSITION DATA

Currently, there appears to be only one data base available for the California desert with day/night resolution of aerosol chemical composition. This is the fine particle data set published by Ouimette (Reference 7). Table 3-2 lists Ouimette's monitoring periods that involved daytime samples immediately prior to or followed by nighttime samples. The table also indicates a plotting notation to distinguish points in subsequent figures.

Ouimette's data base contains seven daytime samples juxtaposed with six nighttime samples. We have calculated an overall average mass balance for these samples as shown in Table 3-3. In agreement with the previously discussed nephelometry data, Table 3-3 shows that the total fine particle mass concentrations are lower during the day than during the night. A mysterious and as yet unexplainable aspect of the data, however, is the rather large "unaccounted for" fine particle mass, which is nearly *identical* in absolute magnitude (5.3 or 5.5 $\mu g/m^3$) for the day and night averages. Expressing the mass balance in terms of "percent of accounted for fine mass" (see values in parentheses) indicates that for Ouimette's overall average data, the particulate chemical composition is essentially identical during day and night. This fact is direct evidence that the particle source mixture does not change radically from day to night, at least on the average.

TABLE 3-2. Sampling Periods for Ouimette's Day/Night Particulate Composition Data.

Typical sampling conditions:

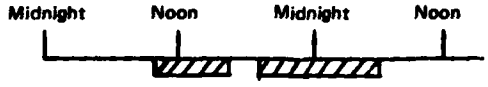

Days and times used:

Type	Day	Start time	Sample length, hrs.
● Day sample followed by night sample	8-06	0900	6
		1900	11
	8-07	0900	6
		1900	11
	8-21	1000	6
		2000	11
	9-05	1000	6
		2110	7.8
	9-06	1210	6.4
		2329	10.3
○ Night sample followed by day sample	8-16,17	2000	11
		0900	7
	9-6,7	2329	10.3
		1100	7
△ Two night samples surrounding a day sample	8-6,7	1900	11
		0900	6
		1900	11
	9-5,6	2110	7.8
		1210	6.4
		2329	10.3

TABLE 3-3. Average Mass Balance of Ouimette's Daytime and Nighttime Fine Particle Samples at China Lake.

Particle	Average mass balance $\mu g/m^3$ (% of accounted for)	
	Day (7 samples), %	Night (6 samples), %
Black carbon (soot)	0.5 (8)	0.7 (7)
Organic C = 1.5 (total C - soot)	1.5 (24)	2.6 (25)
Sulfate	2.0 (32)	2.9 (28)
Nitrate	0.1 (2)	0.2 (2)
Ammonium	0.6 (10)	1.0 (10)
Crustal = ½(4.2 Si + 21.6 Fe)	1.4 (22)	2.6 (25)
K and Pb	0.2 (3)	0.3 (3)
Unaccounted for	5.3	5.5
Total	11.6	15.8

To investigate the data for individual sampling days, Figure 3-11 plots daytime values (similar to 8-hour samples) versus daytime and nighttime averages (similar to 24-hour samples) for various chemical constituents. The plotting notation is explained in Table 3-2. Figure 3-11 reveals that on individual days, the daytime data are often much different from the overall day and night averages. There are two potential explanations. First, the particle source mixtures may vary greatly from day to night on individual days even though they do not vary much in an overall average sense. This variation would support the need to consider shorter sampling times for RESOLVE particulate measurements. Alternatively, the scatter in Figure 3-11 may represent imprecision in the individual measurements. Such imprecision does not appear unlikely given the short sampling periods used by Ouimette and the subsequent lack of large deposits on the particle filters. This would argue the need for 24-hour samples to obtain adequate filter deposits. We are not sure which effect is most pronounced. The real answer may be a combination of both factors, although our study of the data leads us to suspect measurement imprecision as the cause of the most obvious anomalies.

3.4 CONCLUSION

In summary, we have seen that important diurnal variations exist in fine particle concentrations. However, the nephelometry data from the RESOLVE program will serve as a continuous measurement of these variations. With respect to source mixtures, the high correlation between 8-hour and 24-hour b_{sp} indicates qualitatively that daytime and 24-hour particulate concentrations are not uncoupled. Furthermore, Ouimette's data set, although only for a few days in one season, suggests that daytime and nighttime particle compositions are the same in an average sense. Because of the general implications of the above analyses, because of procedural difficulties and extra expenses associated with short-term particulate sampling, and because of some interest in nighttime as well as daytime visibility for DOD operations, it seems most prudent at this time to begin the *routine* RESOLVE program with 24-hour particulate sampling.

It is recommended, however, that further measurements be taken and analyzed to check this conclusion. The drum sampler data for the RESOLVE program will provide routine measurements of time-resolved particulate composition with respect to soil elements and sulfur. Furthermore, as part of the special intensive studies for RESOLVE, the particulate samplers will be run on a daytime and nighttime basis. By analyzing the drum sampler data and the special study data, it should be possible to settle the issue of 8-hour versus 24-hour sampling with more certainty. If it is found that, counter to our current expectations, the particle source mixtures do vary significantly from day to night, then the sampling protocol may be changed later in the program to provide definitive data characterizing this effect.

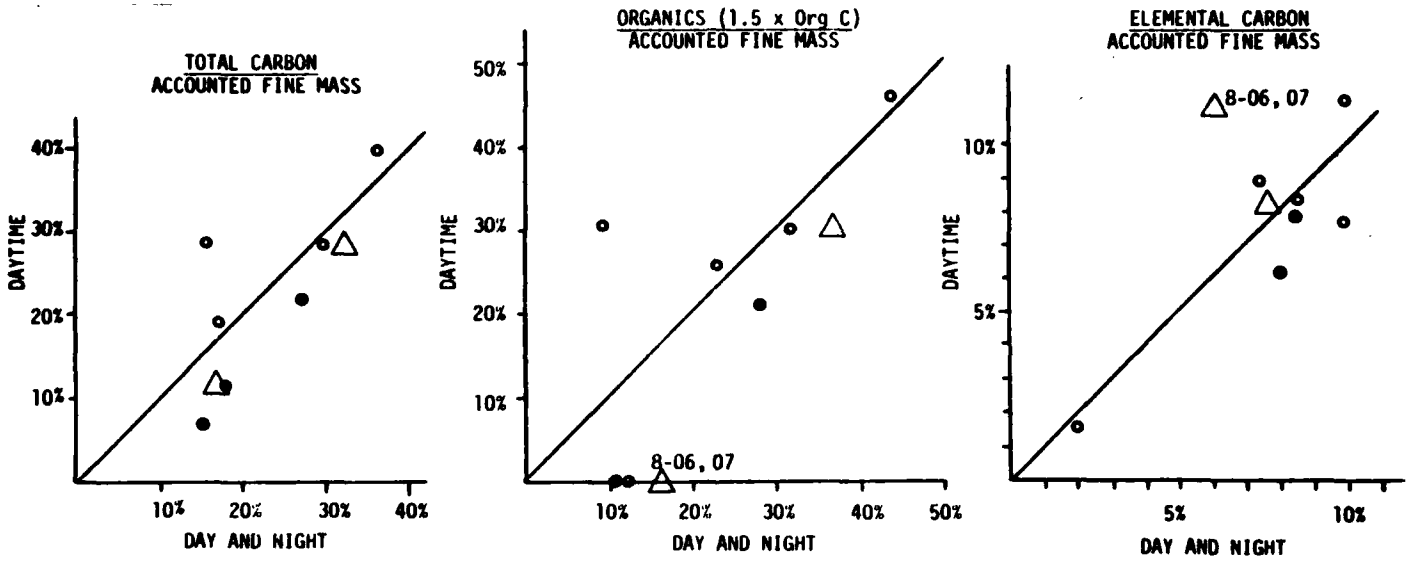

FIGURE 3-11. Daytime Particulate Composition Versus Daytime and Nighttime Average Particulate Composition on Ouimette's Data.

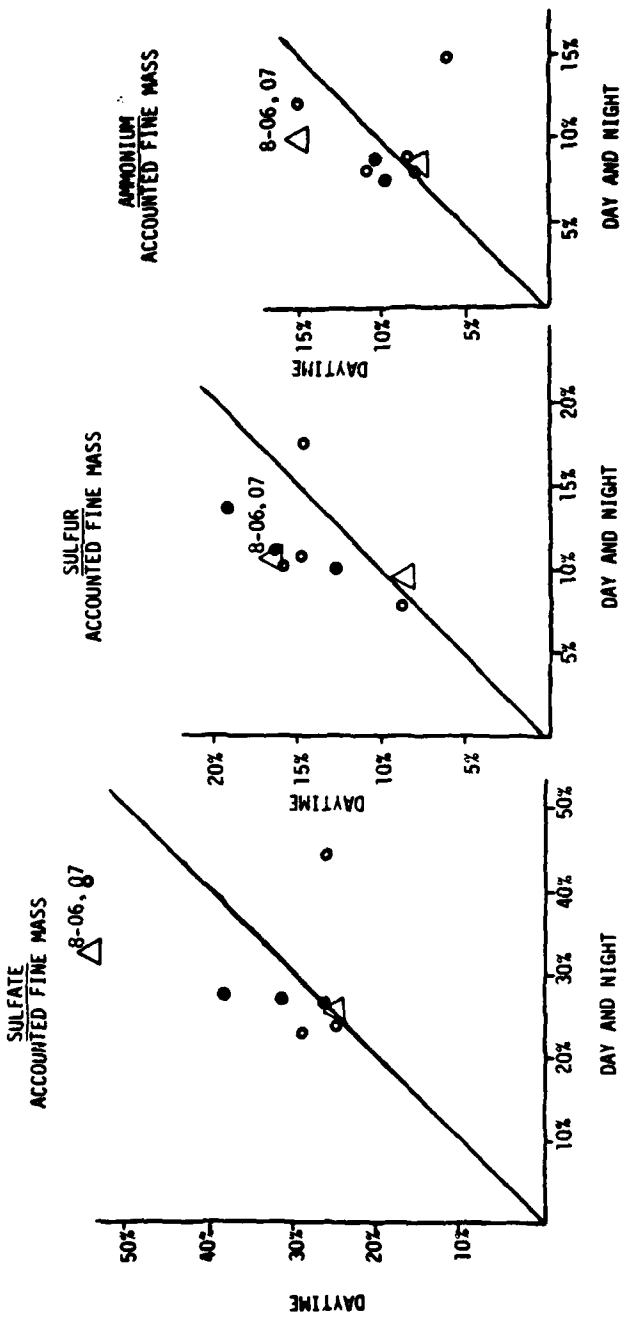

FIGURE 3-11. (Contd.)

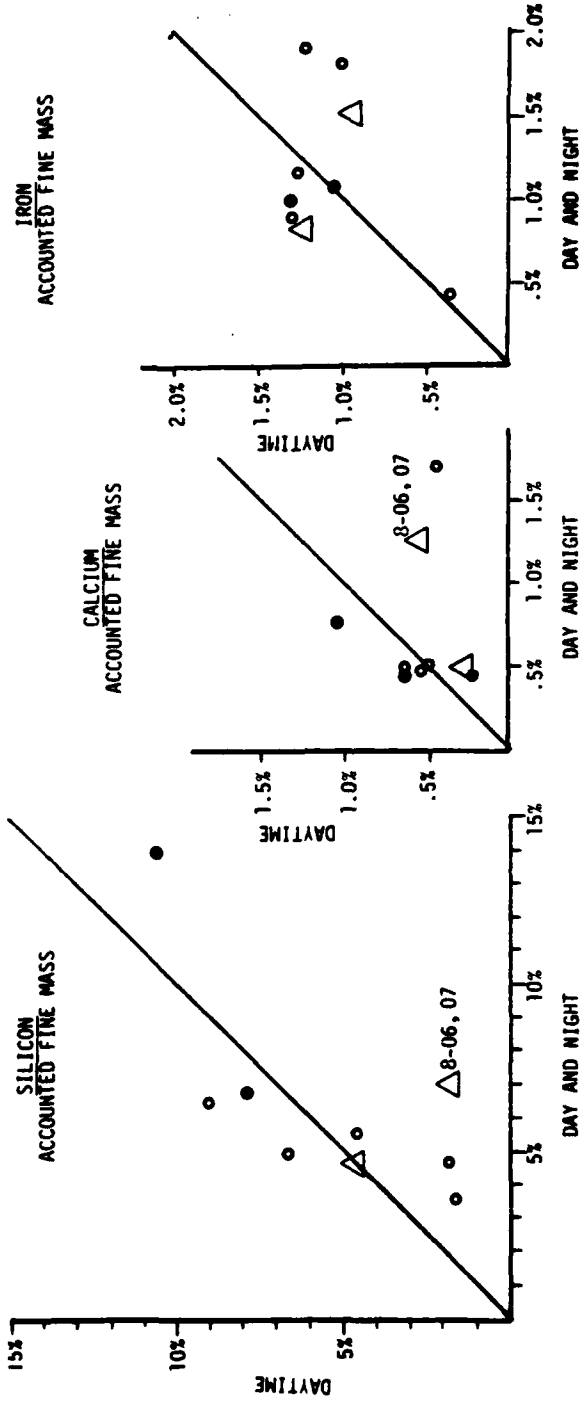

FIGURE 3-11. (Contd.)

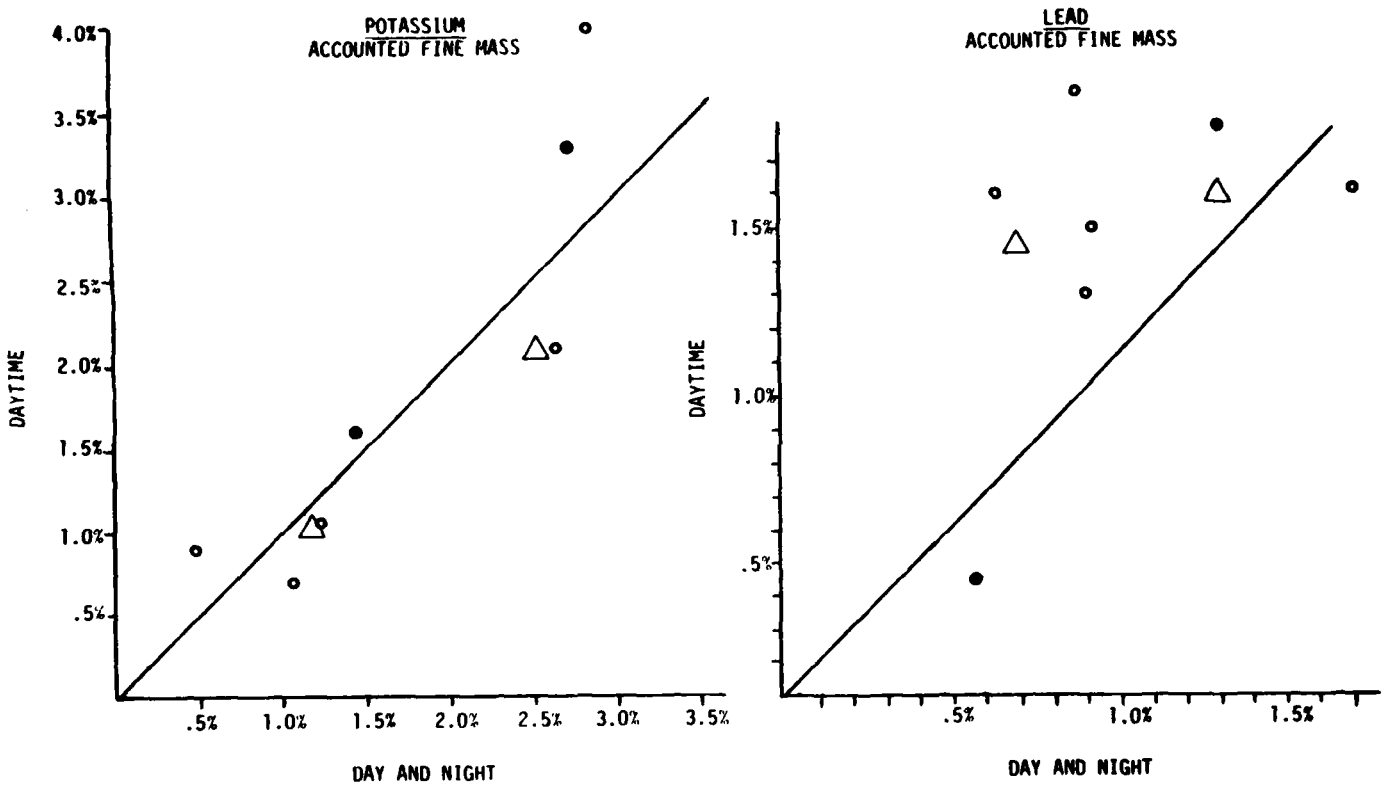

FIGURE 3-11. (Contd.)

4.0 ERROR ANALYSIS OF MASS BALANCE AND PARTICLE SCATTERING BUDGET MODELS FOR RESOLVE

The RESOLVE network intends to quantify the contributions of particle emitting sources to the extinction of light in the atmosphere. This quantification is to be accomplished via the simultaneous measurement of particulate chemical concentrations, light scattering, and light absorption. The contribution of each chemical species to the light scattering is determined by a least squares solution to a set of overdetermined equations expressing the scattering coefficient as a linear combination of the chemical concentrations. This model is termed the "particle scattering budget." When the light absorption due to elemental carbon is added, the model becomes an "extinction budget."

Source contributions to the various chemical species are similarly determined by a least squares solution of simultaneous equations expressing the chemical concentrations as linear sums of the source contibutions. This model is termed the "mass balance."

The results obtained from these calculations will have a degree of uncertainty arising from two components: measurement uncertainty and model uncertainty. Measurement uncertainty results from the imperfection with which any measurement quantifies the true value of a variable. It is expressed as an interval around a nominal value for that variable. If these intervals are known for the measured values given to a model, they can be combined to give an estimate of the measurement uncertainty of the model results.

Model uncertainty result: from the inability of the mathematical model to represent reality. Where the discrepancies between the model and reality can be identified and quantified, it is possible to assign a value to model uncertainties in various applications.

The treatment given here deals with the random measurement uncertainties of the mass balance and particle scattering budget receptor models. Its objectives are:

1. To derive analytical error propagation schemes for calculating the measurement uncertainty of results from the mass balance and particle scattering budget models.

2. To calculate model results and their measurement uncertainties and verify them by repeated calculations using randomly perturbed input data.

3. To estimate the uncertainties of mass balance and scattering budget model predictions as a function of the uncertainty level of model input measurements.

Owing to financial constraints, the scope of this project was severely limited and it cannot answer all questions regarding measurement and model uncertainties in RESOLVE. Several of the most important questions that can be answered by following this methodology will be posed at the end of this treatment.

4.1 DERIVATION OF UNCERTAINTY FORMULAE

The same solution method is used for both mass balance and particle scattering budget models.

The mass balance receptor model is

$$\bar{C}_i = \sum_{j=1}^{p} \bar{a}_{ij} S_j, \quad i=1,n \tag{1}$$

where

$\bar{C}_i$ = exact receptor concentration of species i

$\bar{a}_{ij}$ = exact fraction of species i in source-type j

n = total number of species

p = total number of source types

The overbars are used to indicate the value in the absence of measurement uncertainty. The measured value will be represented by the same symbol without the overbar. If p is less than n, and C_i and a_{ij} are measured with their corresponding uncertainties σ_{C_i} and $\sigma_{a_{ij}}$, then the set of equations (1) can be solved for the most probable values of S_j by minimizing

$$\chi^2 = \sum_{i=1}^{n} \frac{(C_i - \bar{C}_i)^2}{\sigma^2_{C_i}} + \sum_{j=1}^{p} \frac{(a_{ij} - \bar{a}_{ij})^2}{\sigma^2_{\bar{a}_{ij}}} + \sum_{i=1}^{n} \lambda_i(\bar{C}_i - \sum_{j=1}^{p} \bar{a}_{ij}S_j) \tag{2}$$

where λ_i represents a set of LaGrange multipliers. The derivation is accomplished by the following steps (References 8 and 9):

1. The derivatives of χ^2 with respect to $\bar{C}_i$, $\bar{a}_{ij}$, λ_i, and S_j are set equal to zero.

2. Equation (1) is expressed as a Taylor's expansion about estimates of $\bar{C}_i$, $\bar{a}_{ij}$, and S_j.

3. The expansion is combined with the derivatives acquired in step 1 to express the most recent estimate in terms of the previous estimate.

4. The calculated S_j values are Taylor expanded about estimates of the unknown true value, $\bar{S}_j$, and the covariance matrix of the $\bar{S}_j$ differences is obtained. The diagonal elements of this matrix are the uncertainties of the source contributions.

This derivation results in the following set of steps to solve the mass balance equations:

1. The initial values of the source contributions are set equal to zero.

$$\vec{S}^0 = \vec{0} \tag{3}$$

$\vec{S}^k$ is a column vector containing the elements S_j^k. The k superscript refers to the iteration number.

2. The effective variance matrix, $\underset{\sim}{V}_e$, is calculated

$$\underset{\sim}{V}_e^k = \underset{\sim}{V}_C + \sum_{j=1}^{p} \underset{\sim}{V}_{A_j}(S_j^k)^2 \tag{4}$$

$\underset{\sim}{V}_C$ is a diagonal matrix containing the $\sigma^2_{C_i}$, the squared uncertainties of the ambient chemical concentrations. $\underset{\sim}{V}_{A_j}$ is a diagonal matrix containing $\sigma^2_{a_{ij}}$, the squared uncertainties of the source compositions for source j.

3. $$\vec{S}^{k+1} = (\underset{\sim}{A}^T(\underset{\sim}{V}_e^k)^{-1}\ \underset{\sim}{A})^{-1}\ \underset{\sim}{A}^T(\underset{\sim}{V}_e^k)^{-1}\ \vec{C} \tag{5}$$

where $\underset{\sim}{A}$ is a nxp matrix with elements a_{ij}, the source composition matrix, and $\vec{C}$ is a column vector containing the measured concentrations, C_i. S^{k+1} is a column vector the (k+1)st iteration of the source contributions.

4. A comparison is made between the (k+1)st and kth estimates of all S_j. If

$$\frac{S_j^{k+1} - S_j^k}{S_j^k} < 0.01,\ j=1,p \tag{6}$$

then the iteration is terminated. If condition (6) is not true, then steps 2, 3, and 4 are repeated until it is true.

5. The covariance matrix of the S_j is

$$\underset{\sim}{V}_S = \left[\underset{\sim}{A}^T\ (\underset{\sim}{V}_e^k)^{-1}\ \underset{\sim}{A}\right]^{-1} \tag{7}$$

The square roots of the diagonal elements of this matrix are σ_{S_j}, the uncertainties of the corresponding S_j.

The assumptions of this model and solution are (Reference 8):

1. Compositions of source emissions are constant over the period of ambient and source sampling.
2. Chemical species do not react with each other; i.e., they add linearly.
3. All sources with a potential for significantly contributing to the receptor have been identified and have had their emissions characterized.
4. The number of sources is less than or equal to the number of chemical species.
5. The source compositions are linearly independent of each other.
6. Measurement errors are random, uncorrelated, and normally distributed.

7. Measured source compositions closely approximate the true source composition, $a_{ij} = \bar{a}_{ij}$.

Similarly, the particle scattering budget model is

$$b_h = \alpha_0 + \sum_{i=1}^{n-1} \alpha_i C_{hi}, \quad h=1, m \tag{8}$$

where the intercept, α_0, represents the residual Rayleigh scattering in the absence of particulate matter, and α_i is the scattering per unit mass or scattering efficiency of species i. A nominal value for Rayleigh scattering is subtracted from each scattering coefficient to obtain b_h. Since this value will not be constant, a small residual of non-particle scattering is expected to remain. m is the number of samples.

If m is greater than n, the overdetermined set of equation (8) can be solved for the α_i using the same procedure followed for the mass balance. The result will be another iterative solution in which

1. The initial values of the scattering efficiencies are set equal to zero.

$$\vec{\alpha}^0 = \vec{0} \tag{9}$$

where $\vec{\alpha}$ is a column vector containing the elements $\alpha_0^k \cdots \alpha_{n-1}^k$. The k superscript refers to the iteration number.

2. $$\underset{\sim}{V}_e^k = \underset{\sim}{V}_b + \sum_{i-0}^{n-1} \underset{\sim}{V}_{C_i} \ (\alpha_i^k)^2 \tag{10}$$

where $\underset{\sim}{V}_b$ is a diagonal matrix of the $\sigma_{b_h}^2$ and $\underset{\sim}{V}_{C_i}$ is a diagonal matrix of the $\sigma_{C_i}^2$ for each species i.

3. $$\vec{\alpha}^{k+1} = (\underset{\sim}{C}^T(\underset{\sim}{V}_e^k)^{-1}\underset{\sim}{C})^{-1}\underset{\sim}{C}^T(\underset{\sim}{V}_e^k)^{-1} \vec{b} \tag{11}$$

where $\underset{\sim}{C}$ is a mxn matrix with C_{h0} set equal to unity to accommodate the constant α_0 term. $\vec{b}$ is a mxl column vector with elements b_h.

4. Equations (10) and (11) are used alternately until

$$\frac{\alpha_i^{k+1} - \alpha_i^k}{\alpha_i^k} < 0.01, \quad i=1, n \tag{12}$$

5. The σ_{α_i} are the square roots of the diagonal elements of

$$\underset{\sim}{V}_\alpha = \left[\underset{\sim}{C}^T(\underset{\sim}{V}_e^k)^{-1} \underset{\sim}{C} \right]^{-1} \tag{13}$$

This model is derived with the following assumptions (Reference 10):

1. Light in a path is scattered by only one particle (i.e., multiple scattering is ignored).
2. All particles are spheres.
3. Each particle has a homogeneous composition.
4. Particle volume is conserved (i.e., particles are not aqueous or solid solutions).
5. The index of refraction for each particle is constant and equal to the volume average refractive index:

$$\bar{M}_r = \frac{1}{V} \sum_{i=1}^{n} V_i M_{ri} \tag{14}$$

where $\bar{M}_r$ is the volume average refractive index, V is the total particle volume, V_i is the volume of particles of species i, and M_{ri} is the refractive index of species i.

6. Mass-normalized chemical species mass size distributions remain constant for all samples.
7. C_{hi} are not significantly correlated with each other between samples.
8. Measurement errors are normally distributed, random, and uncorrelated.

4.2 MEASUREMENT UNCERTAINTY VERIFICATION

The analytical expressions for measurement error expressed in Equations 7 and 13 can be verified by simulating repeated applications of the measurement process, applying each model to the set of simulated measurements, and calculating the standard deviation of the model results. This procedure is described in detail by Watson (Reference 11). The analytical uncertainties obtained from Equations 7 and 13 should not significantly differ from these standard deviations if they are correct.

The advantage of a simulated test over the use of real measurements is that the model uncertainty can be set equal to zero and the true measurement uncertainties can be precisely known. Figures 4-1 and 4-2 illustrate the simulation process which is followed for these tests. These figures will be referred to in the discussions below.

4.2.1 Mass Balance Verification

Source types which could contribute to particle concentrations in the RESOLVE monitoring region and their compositions are presented in Table 4-1. Ammonium sulfate is a likely secondary product of sulfur dioxide emissions, and much of this gas is released in the oil fields of the lower San Joaquin Valley. The fractional compositions of sulfate, nitrate, and ammonium in these sources were derived from their stoichiometric ratios. Windblown dust is considered to be a major contributor in a desert environment. Field burning is common in California's Central Valley and it is possible that some of its smoke could intrude into the California desert. Numerous roads passing through the region can add motor vehicle exhaust to that which is transported from nearby and distant urban areas. The source compositions for dust, burning, and motor vehicle exhaust in Table 4-1 were drawn from Watson (Reference 11) and may not be totally representative of the California desert. These source compositions are adequate for the purposes of this study, however.

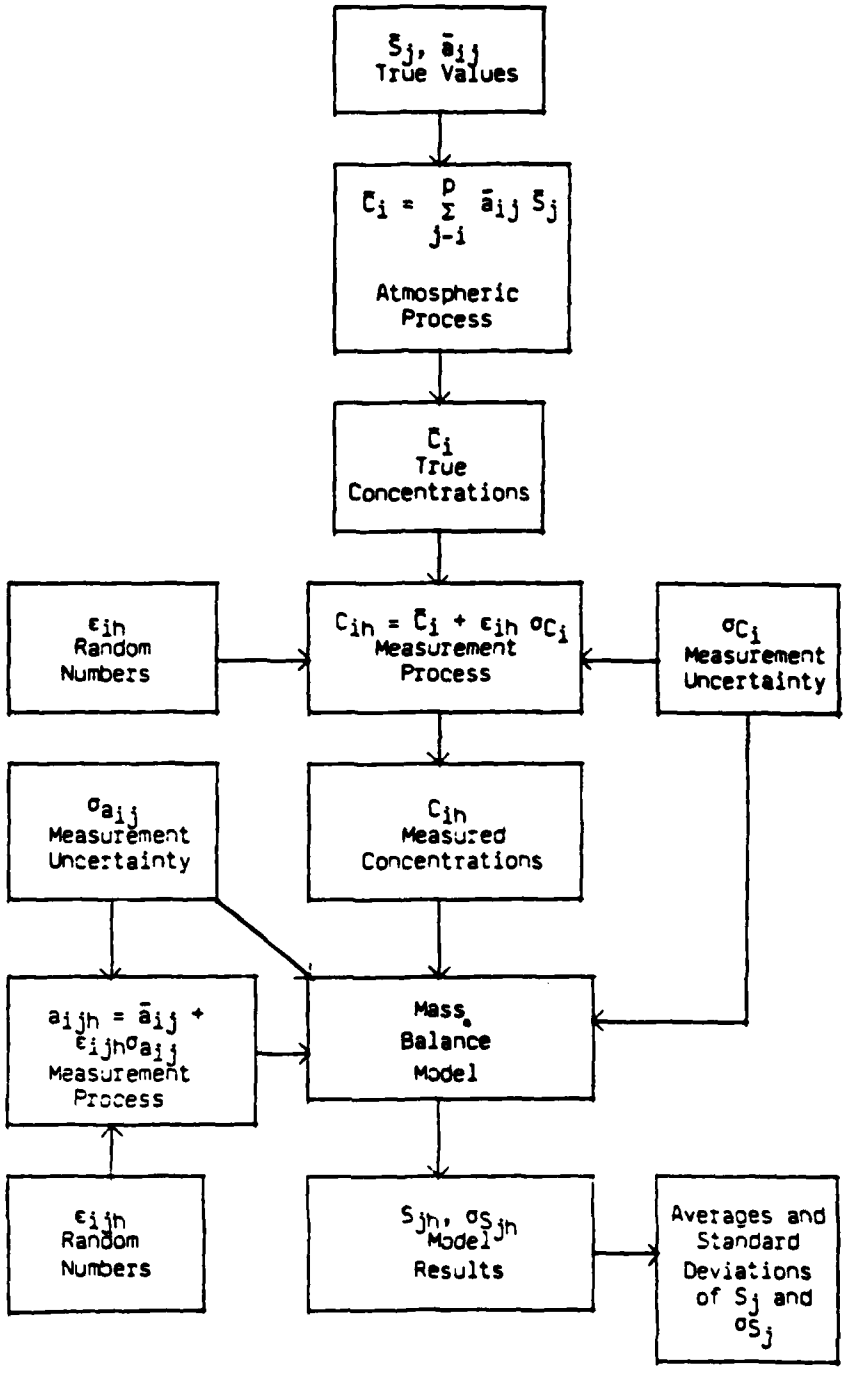

FIGURE 4-1. Process for Verifying Mass Balance Models.

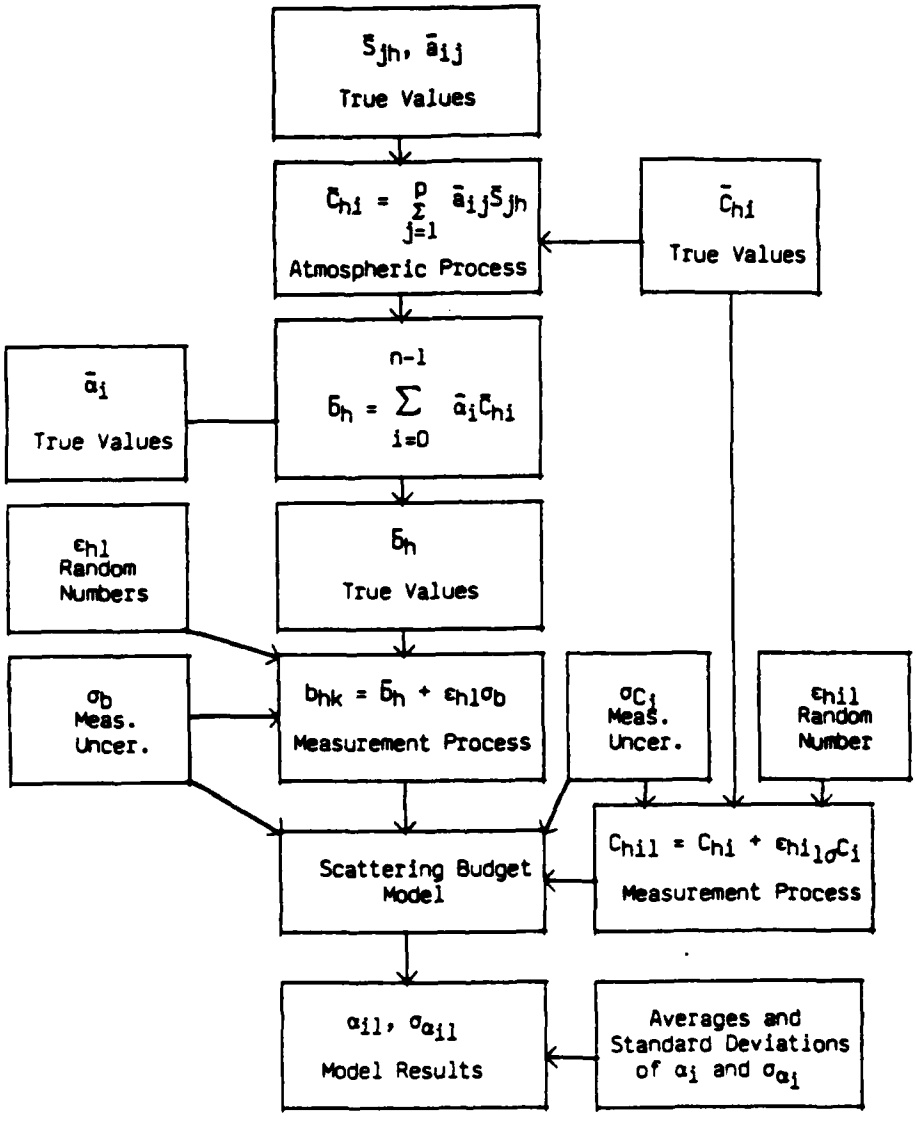

FIGURE 4-2. Process for Verifying Scattering Budget Models.

TABLE 4-1. Fractional Fine Particle Compositions of Five Source Types Which Could Contribute to Ambient Concentrations in China Lake.

Case	Species	Source types				
		NH_4NO_3	$(NH_4)_2SO_4$	Soil	Burning	Mot. veh.
1	Mass	1.000	1.000	1.0000	1.0000	1.0000
2	Organic C	0.000	0.000	0.0430	0.4700	0.5000
3	Graphite C	0.000	0.000	0.0060	0.0400	0.0400
4	NH_4	0.225	0.273	0.0000	0.0000	0.0000
5	NO_3	0.775	0.000	0.0000	0.0200	0.0090
6	SO_4	0.000	0.727	0.0000	0.0500	0.0130
7	Al	0.000	0.000	0.1170	0.0050	0.0110
8	Si	0.000	0.000	0.2540	0.0050	0.0080
9	Cl	0.000	0.000	0.0000	0.0100	0.0300
10	K	0.000	0.000	0.0100	0.0650	0.0070
11	Ca	0.000	0.000	0.0090	0.0090	0.0120
12	Ti	0.000	0.000	0.0080	0.0007	0.0000
13	V	0.000	0.000	0.0003	0.0000	0.0000
14	Cr	0.000	0.000	0.0003	0.0001	0.0000
15	Mn	0.000	0.000	0.0020	0.0005	0.0000
16	Fe	0.000	0.000	0.0680	0.0005	0.0210
17	Ni	0.000	0.000	0.0000	0.0000	0.0002
18	Cu	0.000	0.000	0.0002	0.0005	0.0007
19	Zn	0.000	0.000	0.0041	0.0000	0.0040
20	Br	0.000	0.000	0.0000	0.0005	0.0500
21	Pb	0.000	0.000	0.0000	0.0000	0.2000

True source contributions of 0.5 $\mu g/m^3$ NH_4NO_3, 4.5 $\mu g/m^3$ $(NH_4)_2$ SO_4, 2.8 $\mu g/m^3$ soil, 3.1 $\mu g/m^3$ burning, and 0.8 $\mu g/m^3$ motor vehicle exhaust were selected since these values would yield ambient chemical concentrations at the high end of the fine particle chemical concentration ranges found at China Lake by Ouimette and Flagan (Reference 10).

As Figure 4-1 shows, these true values of $\bar{a}_{ij}$ and $\bar{S}_j$ were linearly combined to obtain true ambient concentrations, $\bar{C}_i$. The measurement process was simulated by adding a random error proportional to the uncertainty of each C_i measurement. Fifty sets of these ambient concentrations were created with uncertainties of 10, 20, and 30% of the $\bar{C}_i$. Similarly, 50 corresponding sets of a_{ij} measurements were produced for uncertainties of 10, 20, and 30% of the $\bar{a}_{ij}$ in Table 4-1. The mass balance model of Equations 3 through 7 was applied to each data set, yielding 50 source contribution values for each source type and uncertainty level. The averages, standard deviations and ranges of the 50 source contributions and their uncertainties were calculated. These results are summarized in Table 4-2 for the three uncertainty levels that were examined.

For each source type, Table 4-2 compares values of the following parameters for 0, 10, 20, and 30% uncertainty levels.

$$\text{Average } S_j = \langle S_j \rangle = \frac{1}{50} \sum_{h=1}^{50} S_{jh} \qquad (15)$$

TABLE 4-2. Averages, Standard Deviations, and Ranges of Source Contributions and Their Uncertainties as a Function of Uncertainty Level.

Source type	Parameter[a]	Uncertainty level			
		0%	10%	20%	30%
1. NH_4NO_3	Average S_j	0.50	0.50	0.51	0.54
	Range of S_j	. . .	0.29 – 0.71	0.26 – 1.0	0.03 – 1.5
	Std. dev S_j	. . .	0.081	0.18	0.30
	Average σ_{S_j}	. . .	0.080	0.17	0.31
	Std. dev σ_{S_j}	. . .	0.013	0.06	0.22
	Range of σ_{S_j}	. . .	0.06 – 0.11	0.09 – 0.32	0.11 – 1.2
	Exact σ_{S_j}	. . .	0.078	0.16	0.23
	Ratio[b]	. . .	1.03	1.13	1.30
2. $(NH_4)_2SO_4$	Average S_j	4.50	4.41	4.34	4.28
	Range of S_j	. . .	3.4 – 6.0	2.5 – 8.0	1.6 – 10.7
	Std. dev S_j	. . .	0.51	1.02	1.56
	Average σ_{S_j}	. . .	0.46	0.92	1.41
	Std. dev σ_{S_j}	. . .	0.05	0.22	0.60
	Range of σ_{S_j}	. . .	0.37 – 0.64	0.64 – 1.9	0.9 – 4.4
	Exact σ_{S_j}	. . .	0.47	0.94	1.40
	Ratio		1.09	1.06	1.11
3. Soil	Average S_j	2.80	2.92	3.09	3.36
	Range of S_j	. . .	1.7 – 3.6	0.90 – 4.9	0.2 – 8.1
	Std. dev S_j	. . .	0.42	0.87	1.46
	Average σ_{S_j}	. . .	0.43	0.91	1.53
	Std. dev σ_{S_j}	. . .	0.05	0.26	0.88
	Range of σ_{S_j}	. . .	0.31 – 0.59	0.52 – 1.9	0.68 – 6.4
	Exact σ_{S_j}	. . .	0.41	0.83	1.24
	Ratio	. . .	1.02	1.05	1.18
4. Burning	Average S_j	3.10	3.24	3.13	3.12
	Range of S_j	. . .	2.4 – 4.0	1.7 – 5.0	0.9 – 6.1
	Std. dev S_j	. . .	0.41	0.79	1.20
	Average σ_{S_j}	. . .	0.39	0.81	1.26
	Std. dev σ_{S_j}	. . .	0.04	0.15	0.37
	Range of σ_{S_j}	. . .	0.34 – 0.48	0.58 – 1.2	0.8 – 2.2
	Exact σ_{S_j}	. . .	0.39	0.79	1.18
	Ratio	. . .	1.05	1.00	1.02
5. Motor vehicle	Average S_j	0.80	0.80	0.79	0.79
	Range of S_j	. . .	0.64 – 1.0	0.50 – 1.3	0.38 – 1.5
	Std. dev S_j	. . .	0.083	0.17	0.26
	Average σ_{S_j}	. . .	0.082	0.17	0.26
	Std. dev σ_{S_j}	. . .	0.010	0.04	0.11
	Range of σ_{S_j}	. . .	0.064 – 0.110	0.10 – 0.31	0.13 – 0.64
	Exact σ_{S_j}	. . .	0.081	0.16	0.24
	Ratio	. . .	1.02	1.06	1.08

[a] All units except those of ratio are $\mu g/m^3$.

[b] $\text{ratio} = \dfrac{\text{std. dev. } S_j}{\text{exact } \sigma_{S_j}}$

The proximity of this average to the 0% uncertainty value verifies that 50 trials provide a valid statistical sample and that the interval within which the perturbed values occur is symmetric. This average is within 10% of the true S_j for all cases except for the 30% uncertainty level for soil. Fifty cases appear to be adequate for statistical purposes.

Range of S_j. The maximum and minimum values of the source contributions calculated from each of the 50 cases estimate the extremes that might be encountered in a single application of the model for each uncertainty level. These extremes differ substantially from the true value, by as much as 40%, even when the measurement uncertainty is as low as 10%. These extremes are within three standard deviations of $\langle S_j \rangle$ in every case, and for 30% uncertainty levels they are within two standard deviations.

$$\text{Standard deviation of } S_j = \sqrt{\frac{1}{49} \sum_{k=1}^{50} (S_{jh} - \langle S_j \rangle)^2} \tag{16}$$

This standard deviation is one representation of the uncertainty of the S_j. If the measurements could be made 50 times, this is the uncertainty that would be calculated. It can be compared to the uncertainty calculated by the application of the model to a single set of measurements.

$$\text{Average } \sigma S_j = \langle \sigma S_j \rangle = \frac{1}{50} \sum_{h=1}^{50} \sigma S_{jh} \tag{17}$$

The analytical uncertainty was calculated by each of the 50 model runs. The average σS_j is within 10% of the standard deviation of S_{jk} in every case.

$$\text{Standard deviation of } \sigma S_j = \sqrt{\frac{1}{49} \sum_{k=1}^{50} (\sigma S_{jk} - \langle \sigma S_j \rangle)^2} \tag{18}$$

When combined with $\langle \sigma S_j \rangle$, this specifies the distribution of the σS_j and shows the extent to which individual values of σS_j will vary owing to measurement uncertainty.

Range of σS_j. The maximum and minimum values of the uncertainties calculated from each of the trials show the extremes which can be reached owing to measurement uncertainties. The maximum and minimum σS_j do not always occur in the same cases as the maximum and minimum S_j. For 10% uncertainty levels, the extremes are within three standard deviations of the average. The extremes are often outside of the three standard deviation interval for 20% and 30% uncertainty levels. For example, the average soil uncertainty at the 30% level is 1.53, but the upper extreme is four times as large.

Exact σS_j. This is the uncertainty that is achieved when the solution is performed with mass balance assumption 7 met exactly. In most of the cases, the errors introduced into the a_{ij} values cause deviations from this assumption with a corresponding over- or under-estimate of the uncertainty.

Ratio of (std. dev. S_j)/(exact σS_j). This ratio should be close to one if the error propagation scheme is working perfectly. This ratio also has a statistical significance as a reduced chi-square statistic with 49 degrees of freedom (one less than the number of cases). With purely random sampling from a normal distribution, as was performed in this study, there is a 50% chance that this ratio will exceed 1.094, a 20% chance that it will exceed 1.163, and a 5% chance that it will exceed 1.350. All ratios in Table 4-2 are reasonably obtainable from random sampling.

The following conclusions can be drawn from the data in Table 4-2:

1. The ability of the mass balance model to calculate the true source contributions degrades as the uncertainty of the input data increases. The standard deviation of the S_j increases nearly proportionately with increases in the measurement uncertainty. For example, the standard deviation of the 50 burning contributions increases from 0.41 to 0.79 to 1.20 as the measurement uncertainty increases from 10 to 20 to 30%.

2. The ability of this model to calculate the uncertainty of the source contributions degrades even more rapidly with increasing measurement uncertainty. For example, the standard deviation of the σS_j for NH_4NO_3 increases fourfold between the 10 and 20% cases, and another fourfold between the 20 and 30% cases. The lower end of the 30% σS_j for NH_4NO_3 range always overlaps the upper end of the 20% σS_j range.

3. When measurement uncertainties are high (i.e., 20 or 30%) the upper extremes of S_j are typically within a factor of two of the true source contribution. The lower extremes can differ by much more than a factor of two. The true source contribution is usually contained within an interval equal to twice the calculated uncertainty for the upper extremes. It is usually outside of this interval for calculated uncertainties associated with the lower extremes. It is impossible to know if one is at these extremes in a single application.

4. The majority of mass balance calculations yield uncertainty estimates such that the true source contribution is within a 3 σS_j interval, and often within a 2 σS_j interval, about the calculated source contribution. For example, a burning contribution of 1.9 $\mu g/m^3$ (one standard deviation less than the average value for the 30% uncertainty level) typically has calculated uncertainty of 0.9. The true 3.1 $\mu g/m^3$ value is within 1.8 $\mu g/m^3$ (2 σS_j) about 1.9 $\mu g/m^3$.

5. The exact σS_j does not differ from the standard deviation of σS_j at a statistically significant level yielded by a chi-squared test. Other values of σS_j, calculated using a_{ij} which differ from $\bar{a}_{ij}$ owing to measurement uncertainty, do differ significantly from the standard deviation of S_j. The range of σS_j shows the extremes in every case.

4.2.2 Scattering Budget Model Verification

The scattering budget model requires ambient chemical concentrations on a number of samples. Twenty-five sets of concentrations were generated from the true source contributions presented in Table 4-1 via equation (1) and the source compositions in Table 4-1. The values in Table 4-3 were chosen to provide ambient chemical concentrations at the low, medium, and high end of the concentrations measured at NWC by Ouimette and Flagan (Reference 10).

These concentrations were combined into the four categories of Ouimette and Flagan:

sulfates = $SO_4^- + NH_4^-$

organics = 1.2 × organic carbon

crustal = 14 × Fe

unaccounted = total mass - sulfates - organics - crustal

TABLE 4-3. Source Contributions to Each Case.

Case	NH_4NO_3	$(NH_4)_2SO_4$	Soil	Burning	Mot. veh.	Comments
1	0.01	1.00	0.90	0.80	0.01	Low concentrations
2	0.25	2.50	1.80	2.30	0.40	Medium concentrations
3	0.50	4.50	2.80	3.10	0.80	High concentrations
4	0.25	2.50	0.90	0.80	0.01	Medium secondary particles dominate
5	0.50	4.50	0.90	0.80	0.01	High secondary particles dominate
6	0.01	1.00	1.80	0.80	0.01	Medium soil dominates
7	0.01	1.00	2.80	0.80	0.01	High soil dominates
8	0.01	1.00	0.90	2.30	0.01	Medium burning dominates
9	0.01	1.00	0.90	3.10	0.01	High burning dominates
10	0.25	2.50	0.90	3.10	0.01	Medium secondary and high burning
11	0.50	4.50	0.90	3.10	0.01	High secondary and high burning
12	0.01	1.00	0.90	0.80	0.40	Medium auto exhaust
13	0.01	1.00	0.90	0.80	0.80	High auto exhaust
14	0.01	1.00	0.90	2.30	0.40	Medium burning and auto exhaust
15	0.01	1.00	0.90	3.10	0.80	High burning and auto exhaust
16	0.25	2.50	1.80	0.80	0.01	Medium secondary and soil
17	0.50	4.50	2.80	0.80	0.01	High secondary and soil
18	0.25	2.50	1.80	0.80	0.40	Medium everything except burning
19	0.50	4.50	2.80	0.80	0.80	High everything except burning
20	0.25	2.50	1.80	2.30	0.01	Medium everything except auto
21	0.50	4.50	2.80	3.10	0.01	High everything except auto
22	0.50	1.00	1.80	2.30	0.40	High nitrate, low sulfate, medium other
23	0.01	4.50	1.80	2.30	0.40	High sulfate, low nitrate, medium other
24	0.50	1.00	2.80	3.10	0.80	High nitrate, low sulfate, high other
25	0.01	4.50	2.80	3.10	0.80	High sulfate, low nitrate, high other

A factor of 14 was chosen for Fe instead of Ouimette and Flagan's factor of 21.6 to make the crustal components consistent with soil source type of Table 4-1 (the inverse of 0.068 is appropriately 14). The total mass for each case was set equal to the sum of the source contributions in each row of Table 4-3.

Exact values for b_{scat} were generated for each of the 25 sets of sulfate, organics, crustal, and unaccounted values plus a small residual according to the formula.

$$b_h = 0.01 + 3.20\ (\text{sulfates})_h + 2.46\ (\textit{organics})h + 1.42\ (\text{crustal})_h + 2.35\ (\text{unaccounted})_h \quad (19)$$

The coefficients of the chemical concentrations are the theoretical values calculated by Ouimette and Flagan. A constant term of 0.01 was chosen to be small compared to the other products. It is of the order of the variation in the Rayleigh scattering coefficient. As Figure 4-2 shows, both the b_h and C_{hi} were submitted to the same randomizing measurement process as before with 10, 20, and 30% uncertainty levels. This is analogous to having three sets of 50 particle samplers and three nephelometers at the same location operating simultaneously for 25 sample periods. One set of samplers and one nephelometer provide data with 10% precision, while the other two sets provide data with 20 and 30% precision, respectively. The results are presented in Table 4-4 and have the same meaning as those reported for the mass balance.

TABLE 4-4. Averages, Standard Deviations, and Ranges of Scattering Efficiencies and Their Uncertainties as a Function of Uncertainty. Unaccounted species are included.

Species	Parameter[a]	Uncertainty level			
		0%	10%	20%	30%
1. Intercept	Average α_i	0.01	0.40	0.79	1.08
	Range of α_i	. . .	−2.0 – 0.71	−3.8 – 4.5	−4.0 – 5.6
	Std. dev α_i	. . .	0.89	1.55	2.10
	Average σ_{α_i}	. . .	0.84	1.49	1.96
	Std. dev σ_{α_i}	. . .	0.08	0.23	0.35
	Range of σ_{α_i}	. . .	0.74 – 1.07	1.19 – 2.21	1.43 – 2.97
	Exact σ_{α_i}	. . .	0.89	1.78	2.67
	Ratio[b]	. . .	1.00	0.87	0.79
2. Sulfates	Average α_i	3.20	3.03	2.74	2.44
	Range of α_i	. . .	2.2 – 3.7	1.1 – 3.9	0.40 – 3.8
	Std. dev α_i	. . .	0.31	0.56	0.75
	Average σ_{α_i}	. . .	0.33	0.58	0.79
	Std. dev σ_{α_i}	. . .	0.02	0.06	0.96
	Range of σ_{α_i}	. . .	0.28 – 0.41	0.49 – 0.78	0.65 – 1.97
	Exact σ_{α_i}	. . .	0.35	0.70	1.05
	Ratio	. . .	0.89	0.80	0.71
3. Organics	Average α_i	2.46	2.03	1.71	1.68
	Range of α_i	. . .	−0.4 – 4.0	−1.3 – 5.6	−2.1 – 5.1
	Std. dev α_i	. . .	1.07	1.57	1.86
	Average σ_{α_i}	. . .	1.31	1.84	2.06
	Std. dev σ_{α_i}	. . .	0.17	0.29	0.34
	Range of σ_{α_i}	. . .	0.95 – 1.55	1.22 – 2.28	1.53 – 2.51
	Exact σ_{α_i}	. . .	1.59	3.19	4.78
	Ratio	. . .	0.67	0.49	0.39
4. Crustal	Average α_i	1.42	1.38	1.41	1.49
	Range of α_i	. . .	0.6 – 2.5	0.0 – 2.5	−0.5 – 3.2
	Std. dev α_i	. . .	0.42	0.75	0.98
	Average σ_{α_i}	. . .	0.46	0.86	1.17
	Std. dev σ_{α_i}	. . .	0.04	0.13	0.20
	Range of σ_{α_i}	. . .	0.38 – 0.55	0.63 – 1.1	0.76 – 1.6
	Exact σ_{α_i}	. . .	0.47	0.94	1.40
	Ratio	. . .	0.89	0.80	0.70
5. Unaccounted	Average α_i	2.35	2.95	3.51	3.65
	Range of α_i	. . .	0.12 – 6.0	−1.8 – 8.3	−2.5 – 11.5
	Std. dev α_i	. . .	1.61	2.42	3.00
	Average σ_{α_i}	. . .	1.96	2.76	3.13
	Std. dev σ_{α_i}	. . .	0.24	0.45	0.57
	Range of σ_{α_i}	. . .	1.29 – 2.3	2.09 – 3.60	1.93 – 4.53
	Exact σ_{α_i}	. . .	2.38	4.76	7.15
	Ratio	. . .	0.62	0.51	0.42

[a] All units except those of ratio are in m^2/g.

[b] $\text{ratio} = \dfrac{\text{std. dev. } \alpha_i}{\text{exact } \sigma_{\alpha_i}}$

Table 4-4 contains several unexpected results. First, the value for the intercept is not accurately reproduced by the least squares solution. Its average increases from a factor of 40 to a factor of 100 over true value as the uncertainty level increases from 10 to 30%. In each of these cases, however, even the minimum σ_{α_i} defines an interval about the intercept value that contains the true value, and usually even surpasses the calculated value of the intercept. The interpretation can usually be drawn that the intercept is not significantly different from zero and should be eliminated from the solution.

The average values for each of the α_i do not approximate the true values nearly as well as they did in the case of the mass balance. For example, the unaccounted $<\alpha_i>$ at the 30% uncertainty level is 55% higher than its true value. This means that 50 samples are not adequate, which is unlikely given the results observed with the mass balance, or that the variability about the average is not symmetric. Many of the low extreme values are negative. Though these are perfectly reasonable solutions to the equation, they are physically impossible.

Finally, the agreement between the exact σ_{α_i} and the standard deviation of α_i is not good. Many of the ratios are significantly less than 1, some being less than 0.5. The uncertainty calculation overpredicts the real variability due to measurement uncertainty.

It is suspected that one or more of the model assumptions is violated by this application, and the most likely one is assumption 7. By definition, the unaccounted variable contains a linear sum of the other variables and must be correlated with them to some extent. To test this hypothesis the randomized data sets were regenerated using the equation

$$b_h = 0.01 + 3.20\ (\text{sulfates})_h + 2.46\ (\text{organics})_h + 1.42\ (\text{crustal})_h \qquad (20)$$

The results are presented in Table 4-5. There are several similarities and differences with respect to Table 4-4. The average intercept is still large compared to the true value, but it is still within the uncertainty interval. The average values of α_i more closely approximate the true value S_i; the maximum differences are 15% for sulfates at the 30% uncertainty level in Table 4-5 and is 24% in Table 4-4. There are fewer negative extreme values for α_i, and where they exist, the σ_{α_i} uncertainty interval associated with them includes values greater than zero. There is close agreement between the exact σ_{α_i} and the standard deviation of α_i as evidenced by the closeness of the ratios to unity. There is probably a minor deviation from assumption 7 in this case owing to the C_{hi} being linear combinations of the same S_{jh}, but this deviation does not appear to be as significant as it might be in the case of Table 4-4.

Conclusions similar to those of the mass balance evaluation can be drawn from Tables 4-4 and 4-5.

1. The model's calculations of the correct α_i and σ_{α_i} become less accurate as the measurement uncertainty increases. In both Tables 4-4 and 4-5 the increase in the standard deviation of α_i is nearly linear, similar to the mass balance. For the unaccounted component in Table 4-4, the standard deviation of α_i does not increase as rapidly with increasing uncertainty; it less than doubles when the uncertainty level increases from 10 to 30%.

2. The standard deviation of σ_{α_i} also increases with increasing measurement uncertainty, but not so rapidly as it did in the mass balance evaluation. For example, in Table 4-4, σ_{α_i} for organics only doubles when the uncertainty level increases from 10 to 30%. It increases by a factor of 6 for the corresponding entry in Table 4-5.

TABLE 4-5. Averages, Standard Deviations, and Ranges of Scattering Efficiencies and Their Uncertainties as a Function of Uncertainty Level. Unaccounted Species are not included.

Species	Parameter[a]	Uncertainty level			
		0%	10%	20%	30%
1. Intercept	Average α_i	0.01	0.15	0.57	1.04
	Range of α_i	. . .	−1.6 – 1.5	−3.0 – 1.0	−3.6 – 5.5
	Std. dev α_i	. . .	0.74	1.41	1.93
	Average σ_{α_i}	. . .	0.72	1.31	1.72
	Std. dev σ_{α_i}	. . .	0.06	0.18	0.30
	Range of σ_{α_i}	. . .	0.63 – 0.87	1.01 – 1.74	0.41 – 2.41
	Exact σ_{α_i}	. . .	0.75	1.50	2.25
	Ratio[b]	. . .	0.99	0.94	0.86
2. Sulfates	Average α_i	3.20	3.14	2.97	2.73
	Range of α_i	. . .	2.8 – 3.9	2.2 – 4.4	1.76 – 4.7
	Std. dev α_i	. . .	0.27	0.53	0.73
	Average σ_{α_i}	. . .	0.25	0.49	0.68
	Std. dev σ_{α_i}	. . .	0.015	0.056	0.10
	Range of σ_{α_i}	. . .	0.23 – 0.30	0.40 – 0.60	0.55 – 0.89
	Exact σ_{α_i}	. . .	0.26	1.00	0.92
	Ratio	. . .	1.04	0.0	0.0
3. Organics	Average α_i	2.46	2.40	2.27	2.14
	Range of α_i	. . .	1.5 – 3.3	0.67 – 3.9	−0.2 – 5.0
	Std. dev α_i	. . .	0.40	0.81	1.19
	Average σ_{α_i}	. . .	0.43	0.80	1.09
	Std. dev σ_{α_i}	. . .	0.03	0.10	0.19
	Range of σ_{α_i}	. . .	0.37 – 0.50	0.61 – 1.11	0.74 – 1.7
	Exact σ_{α_i}	. . .	0.44	0.89	1.33
	Ratio	. . .	0.91	0.91	0.89
4. Crustal	Average α_i	1.42	1.40	1.38	1.38
	Range of α_i	. . .	0.68 – 2.41	0.0 – 3.3	−0.2 – 4.1
	Std. dev α_i	. . .	0.41	0.79	1.10
	Average σ_{α_i}	. . .	0.40	0.75	1.01
	Std. dev σ_{α_i}	. . .	0.04	0.13	0.23
	Range of σ_{α_i}	. . .	0.36 – 0.49	0.48 – 1.04	0.59 – 1.57
	Exact σ_{α_i}	. . .	0.42	0.84	1.26
	Ratio	. . .	0.98	0.94	0.87

[a] All units except those of ratio are in m^2/g.

[b] $\text{ratio} = \dfrac{\text{std. dev. } \alpha_i}{\text{exact } \sigma_{\alpha_i}}$

3. The upper extremes of S_i calculations at 30% uncertainty levels always exceed the true value by a factor of 2, except for sulfate, in both Tables 4-4 and 4-5. The lower extremes are not significantly different from zero, except for sulfate. This is also the case for uncertainty levels of 20% when unaccounted species are included. There is a reasonable chance that this model may substantially over- or under-predict the true values when measurement uncertainties exceed 20%.

4. For the majority of the cases at all uncertainty levels, the true value falls within an interval equal to $2\sigma_{\alpha_i}$ or $3\sigma_{\alpha_i}$ about the calculated value.

5. The exact uncertainties calculated by the model which includes unaccounted species overestimate the standard deviation of α_i by a substantial amount. The exact σ_{α_i} do not significantly differ from the standard deviations of α_i when the unaccounted species do not contribute to the scattering and are not included in the model.

4.3 FURTHER ERROR ANALYSIS

This study has dealt only with a limited case and its results may not be applicable to every case in the RESOLVE program. It has also confined itself to measurement uncertainty and has not examined the effects of model uncertainty; i.e., the effects of deviations from model assumptions. The methodology described here is perfectly applicable to the evaluation of model as well as measurement uncertainty.

As RESOLVE progresses, this type of analysis should be made an integral part of the data interpretation process. After the first mass balances and extinction budgets have been performed, the calculated source contributions and extinction efficiencies should be used as the true values to generate the randomized data sets. This will allow general conclusions to be drawn from cases which are more representative of the actual situation than the hypothetical example used in this study.

Known deviations from each of the model assumptions should be introduced into the simulated data generation scheme. The most important tests for the mass balance model are

1. **Test of Assumption 5.** The similarity of source compositions that can still be resolved by the mass balance model can be determined by making successive calculations in which the compositions become more equal to each other. Regional aerosol composition patterns, which are normally very similar, can be evaluated as pseudo-sources to determine the contributions of various source regions to the receptors.

2. **Test of Assumption 2.** Nonlinear interactions, particularly those involved in the formation of secondary aerosol, can be introduced into the randomized data generation scheme. Deviations from this assumption relate to the accuracy with which primary and secondary sulfate, nitrate, and organic material can be apportioned.

3. **Test of Assumption 3.** The randomized data can be generated with a greater or lesser number of sources than are included in the solution. This will determine the likelihood of missing a source which is really there or identifying contributions from a nonexistent source.

For the scattering budget model, the following tests are important:

1. **Test of Assumption 2.** The true scattering efficiencies of randomly oriented spherical particles should be calculated and compared to the spherical values. If the differences between them are smaller than the typical uncertainties calculated by the scattering budget model, then this assumption can be relaxed.

2. **Test of Assumption 6.** The scattering efficiencies of various size distributions should be used to generate the randomized data. The variability of the model results owing to this deviation can then be quantified and compared to the uncertainties to judge its significance.

3. **Test of Assumption 7.** Known correlations of increasing magnitudes can be introduced into the independent variables. This test may resolve the curiosities observed when the unaccounted species were included in the model.

4.4 CONCLUSIONS

Least squares solutions to the mass balance and scattering budget receptor models have been derived that provide uncertainty estimates for model results. These uncertainties are functions of the uncertainties of both the dependent and independent variables in the models. Applications of these models to randomized data derived from known source contributions and known scattering efficiencies show that the calculated uncertainties are good estimates of the real uncertainties, even when the measurement uncertainty levels are as high as 30%. To characterize and minimize the uncertainty of the interpretive analysis results, the RESOLVE program should document and minimize the measurement uncertainties and maximize the number of sampling cases. The latter would allow multiple applications of statistical models for various data subjects.

REFERENCES

1. B. R. Appel and others. *Visibility Reduction as Related to Aerosol Constituents*, final report under Agreement No. ARB A1-081-32, prepared for the Research Division of the California Air Resources Board, Sacramento, Calif., October 1983.

2. A. Davidson. *Visibility in the South Coast Air Basin: Patterns, Relationship to Particulate Concentrations, and Trends*, presented at the annual meeting of the West Coast Chapter of the Air Pollution Control Association, Scottsdale, Ariz., 26 October 1983.

3. J. Trijonis and others. *Analysis of Visibility/Aerosol Relationships and Visibility/Monitoring Alternatives for California*, final report under Contract No. A9-103-31, prepared for the California Air Resources Board, Sacramento, Calif., February 1982.

4. D. Lehrman and others. *Impact of Transport from South Coast Basin on Ozone Levels in the SE Desert Air Basin*, Vol. 4, MRI Report to California Air Resources Board DV-1871, 1982.

5. J. Trijonis. "Visibility in California," *J. of the Air Poll. Contr. Assn.*, Vol. 32, No. 2 (1982), pp. 165-69.

6 Hegg. "Personal Communication," data from University of Washington cloud physics aircraft, funded by Southern California Edison, 1983.

7. J. R. Ouimette. "Aerosol Chemical Species Contributions to the Extinction Coefficient," Ph. D. Thesis, California Institute of Technology, Pasadena, Calif., 1981.

8. J. G. Watson, J. A. Cooper, and J. J. Huntzicker. "The Effective Variance Weighting for Least Squares Calculations Applied to the Mass Balance Receptor Model," accepted by *Atmos. Environ.*, 1984.

9. H. I. Britt and R. H. Luecke. "The Estimation of Parameters in Nonlinear, Implicit Models," *Technometrics*, Vol. 15 (1973), pp. 233-47.

10. J. R. Ouimette and R. C. Flagon. "The Extinction Coefficient of Multi-Component Aerosols," *Atmos. Environ.*, Vol. 16 (1982), pp. 2405-19.

11. J. G. Watson. "Chemical Element Balance Receptor Model Methodology for Assessing the Sources of Fine and Total Suspended Particulate Matter in Portland, Oregon," Ph. D. dissertation, Oregon Graduate Center, Beaverton, Ore., 1979.

Appendix A

MONTHLY DIURNAL PATTERNS IN PARTICLE SCATTERING FOR FIVE CALIFORNIA DESERT SITES

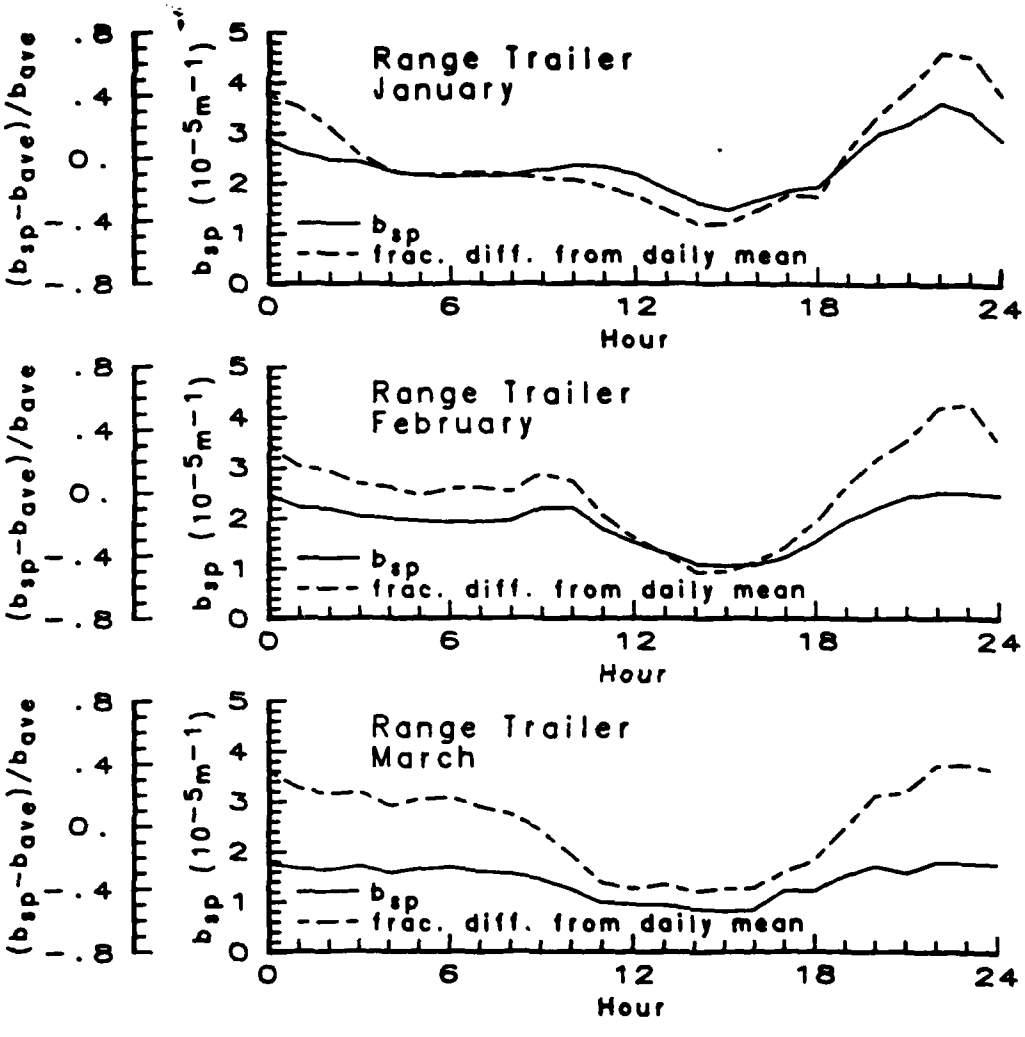

FIGURE A-1. Monthly Diurnal Patterns of Particle Scattering at China Lake Range Trailer.

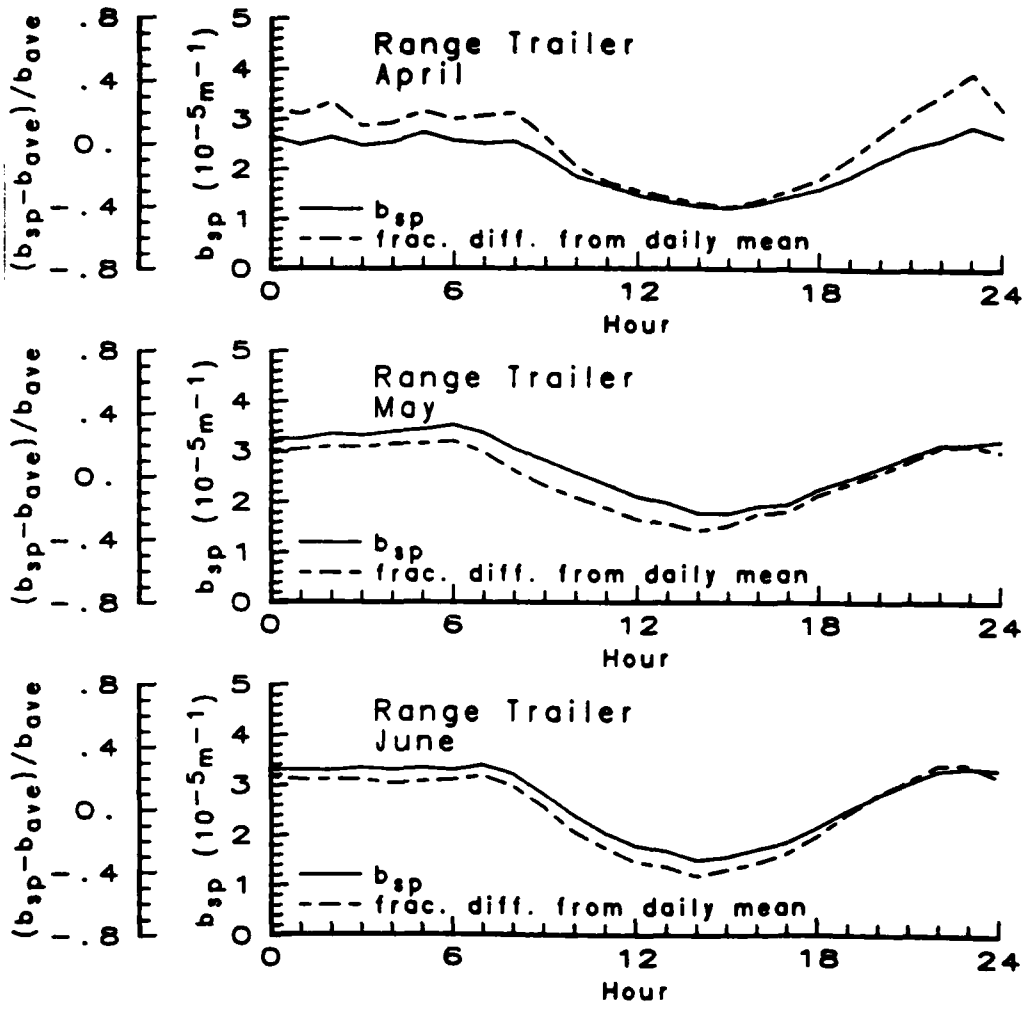

FIGURE A-1. (Contd.)

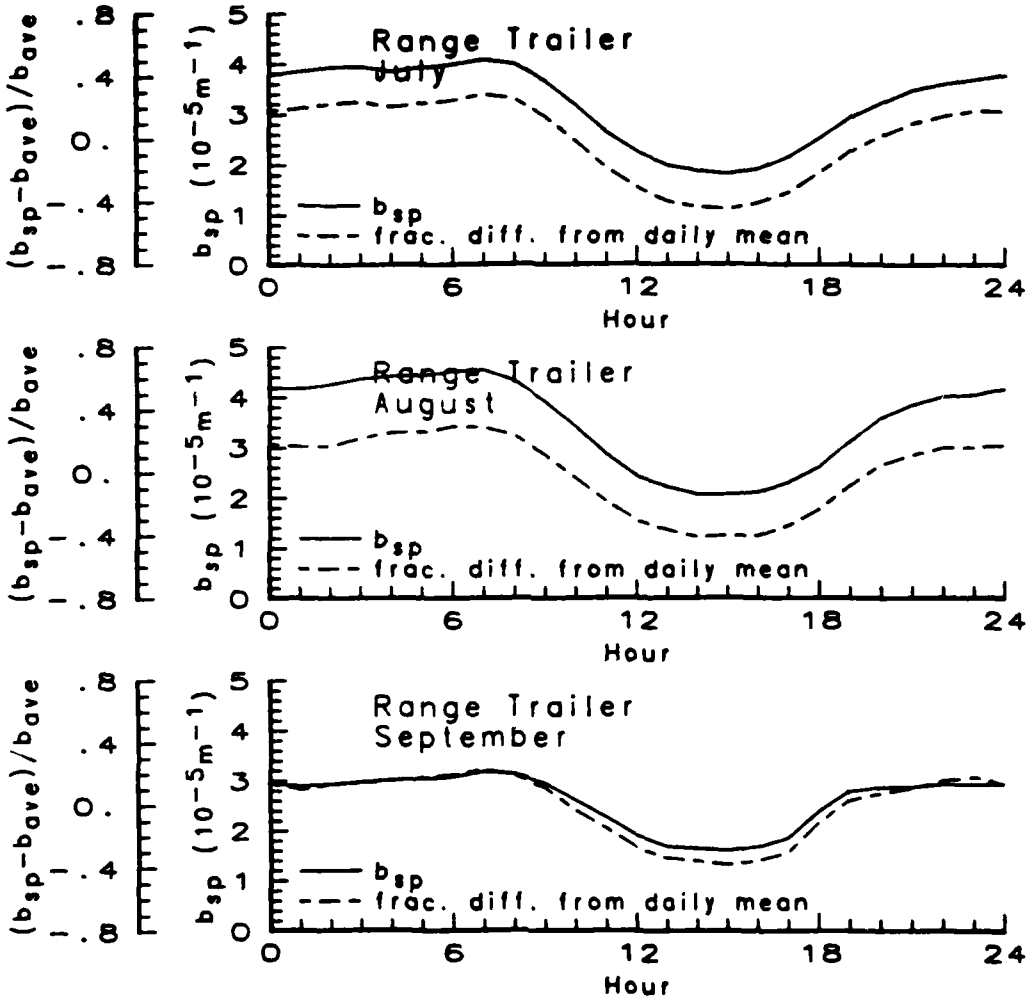

FIGURE A-1. (Contd.)

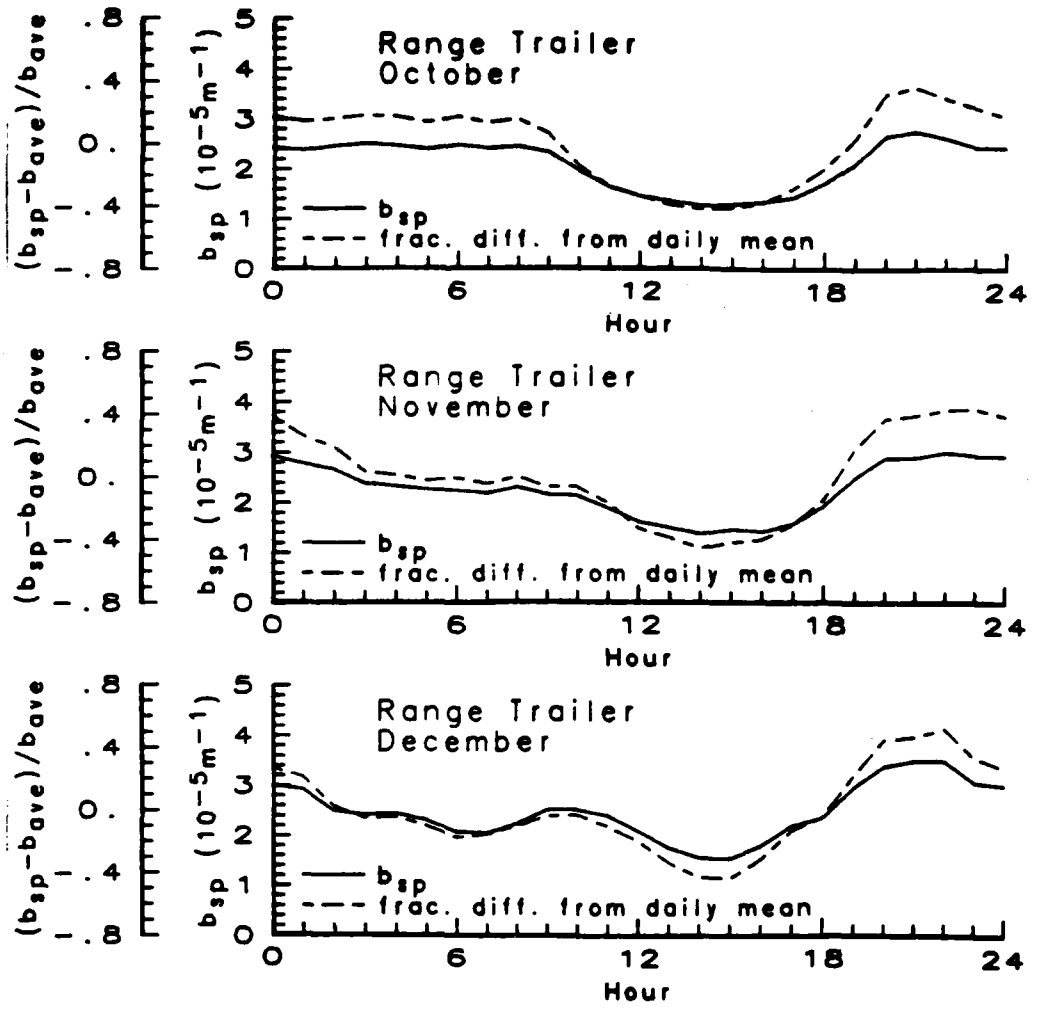

FIGURE A-1. (Contd.)

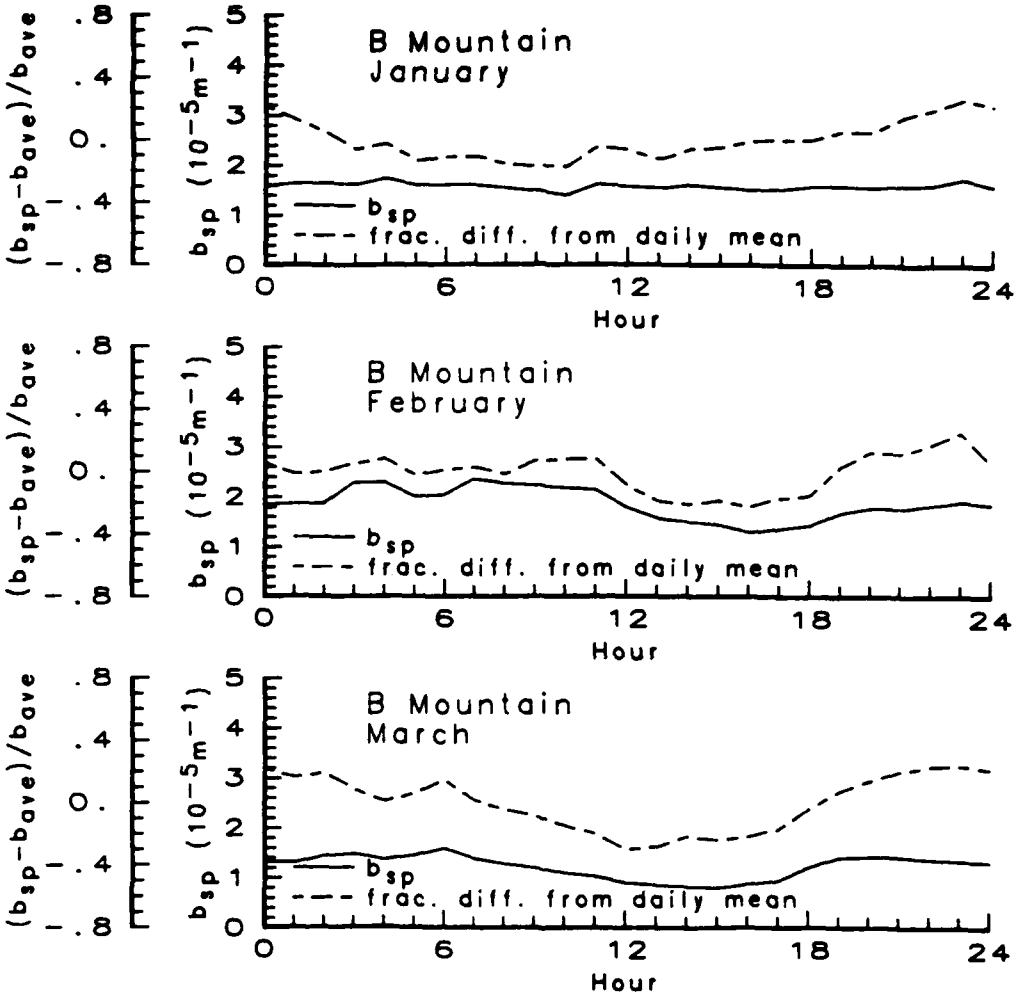

FIGURE A-2. Monthly Diurnal Patterns of Particle Scattering at China Lake B Mountain.

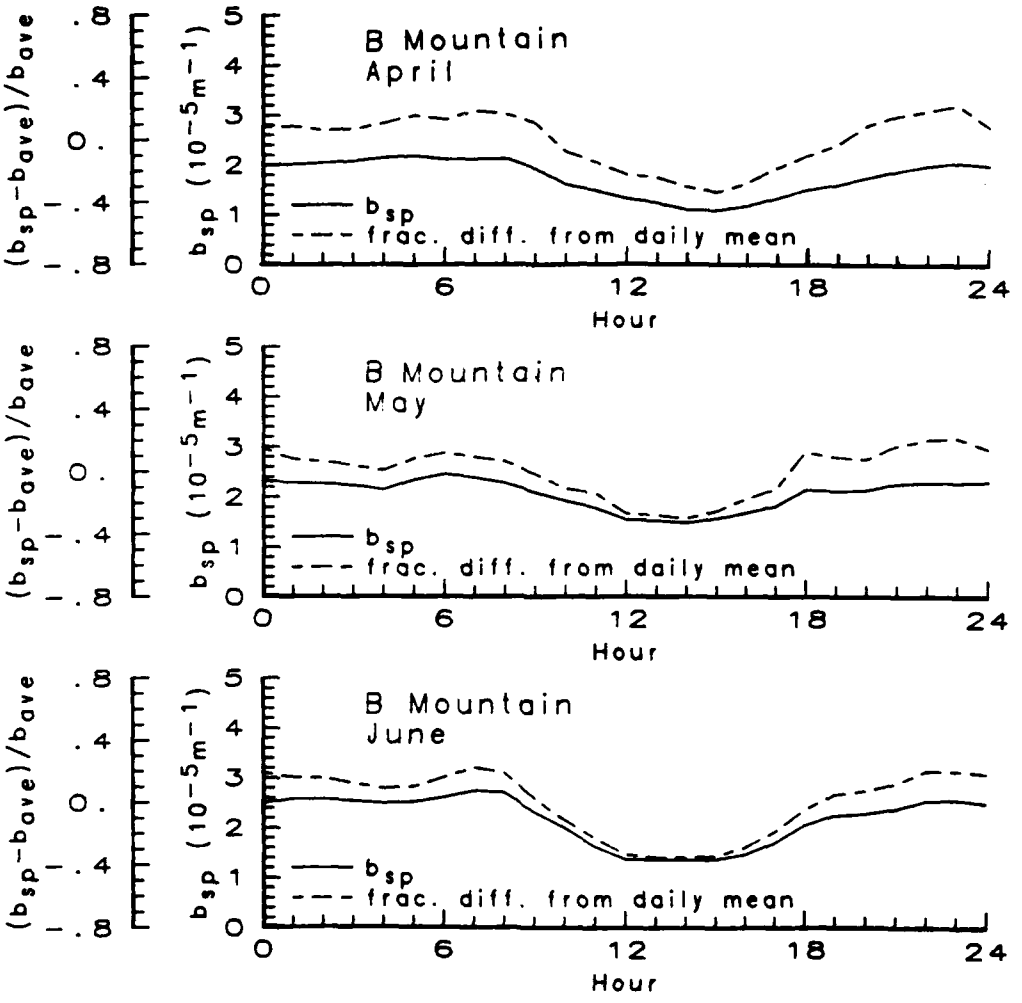

FIGURE A-2. (Contd.)

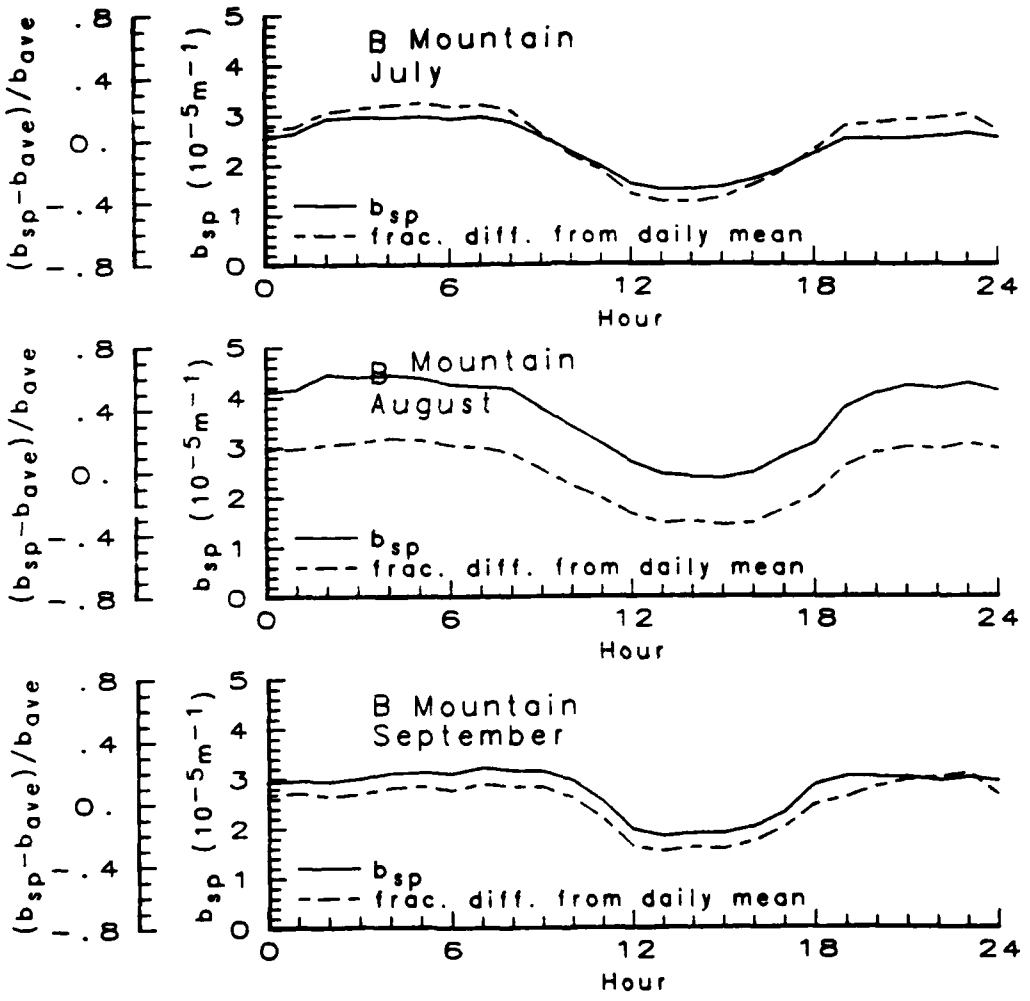

FIGURE A-2. (Contd.)

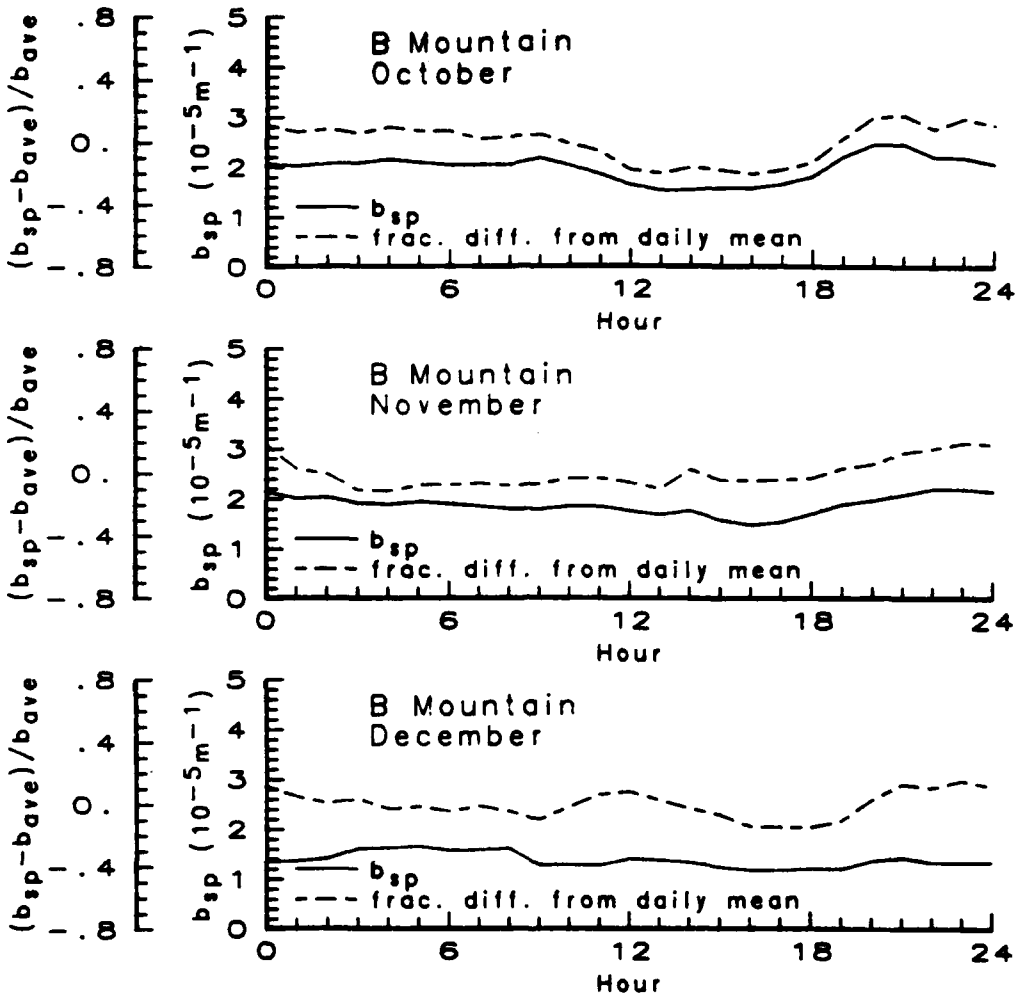

FIGURE A-2. (Contd.)

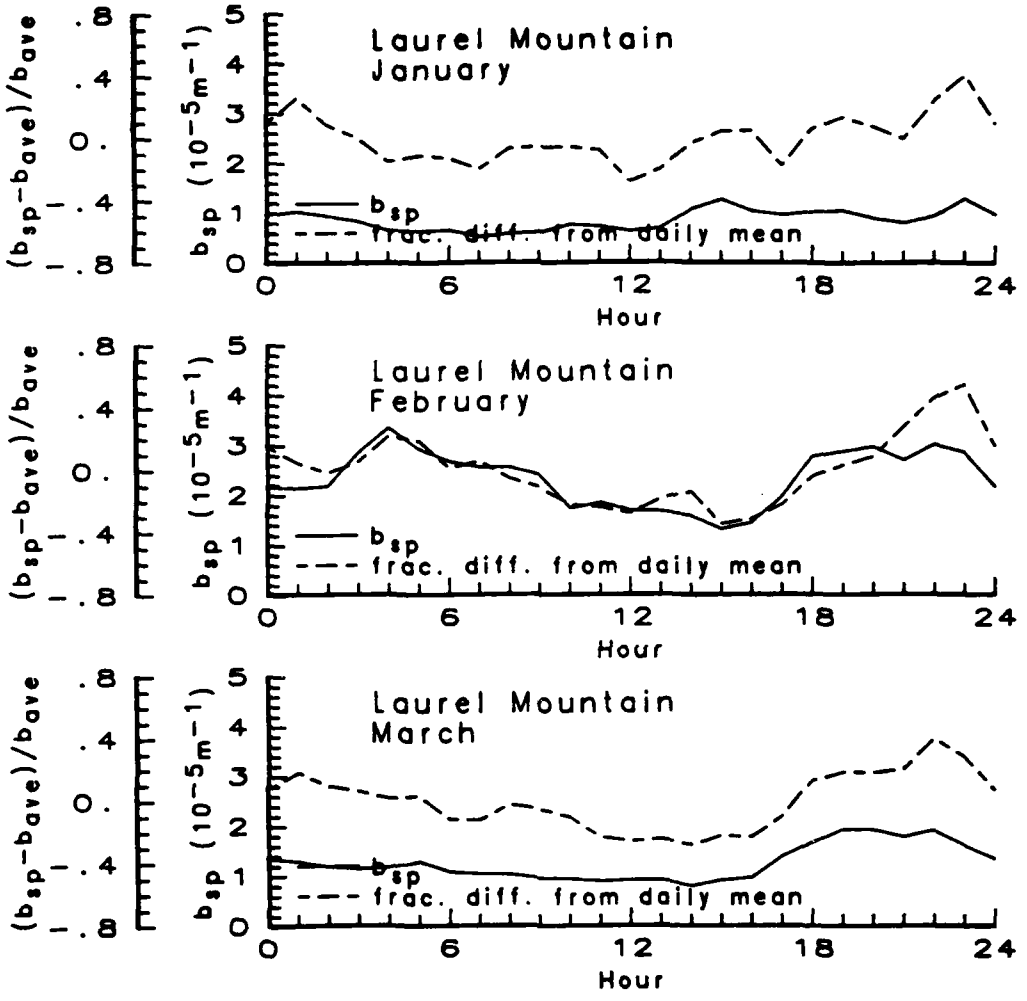

FIGURE A-3. Monthly Diurnal Patterns of Particle Scattering at Laurel Mountain.

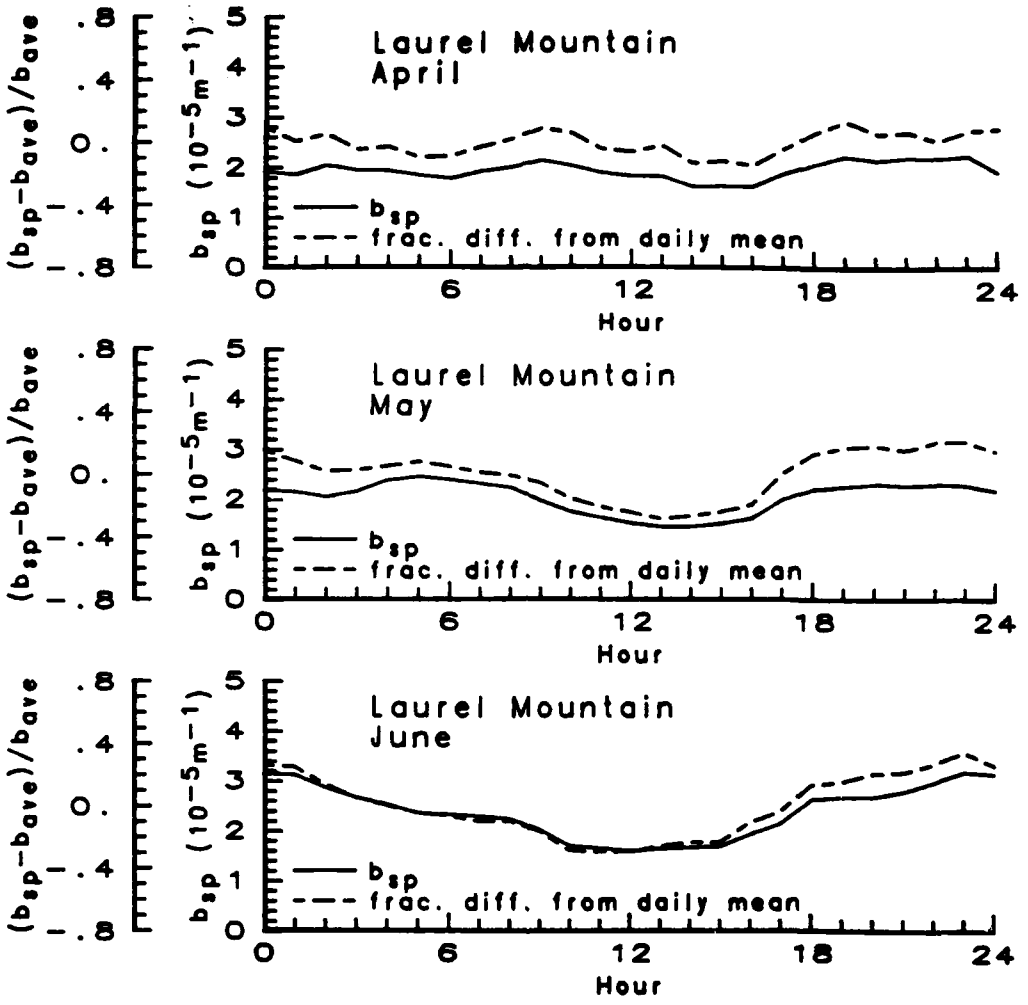

FIGURE A-3. (Contd.)

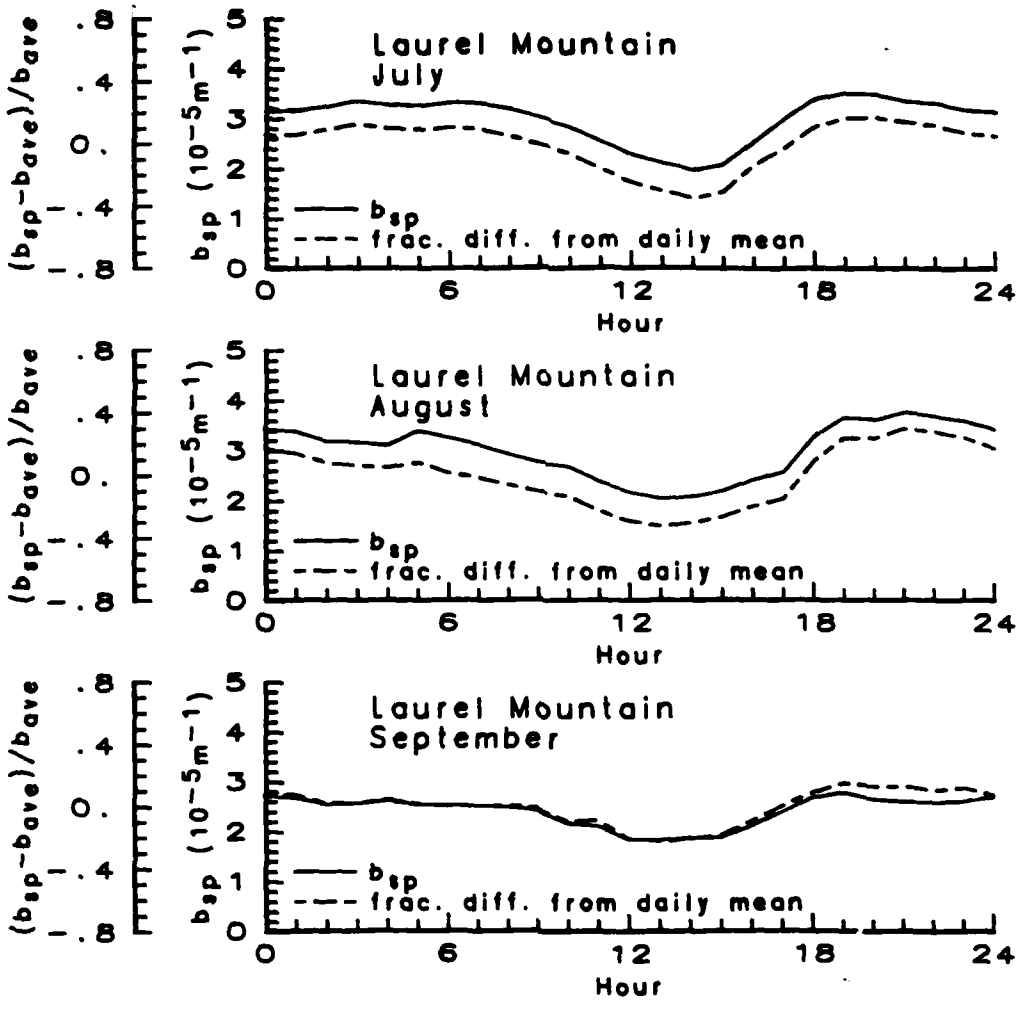

FIGURE A-3. (Contd.)

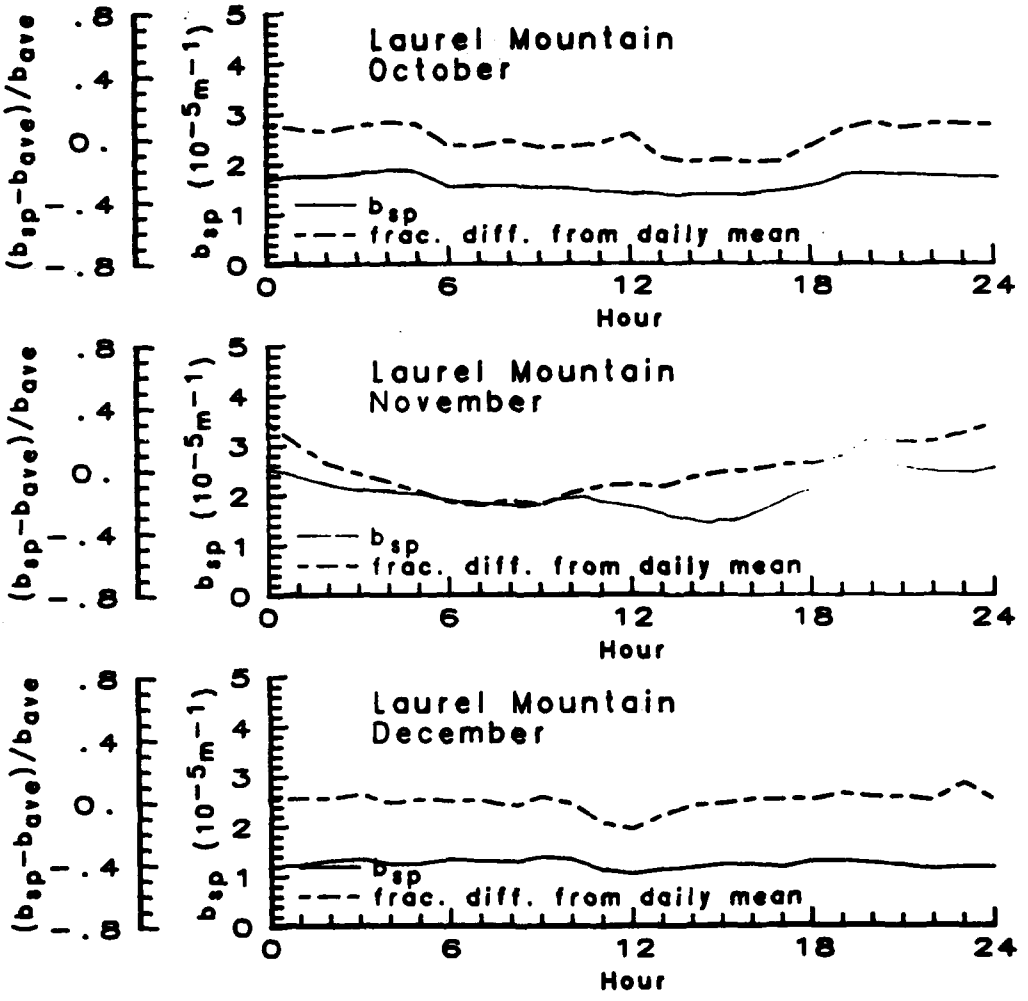

FIGURE A-3. (Contd.)

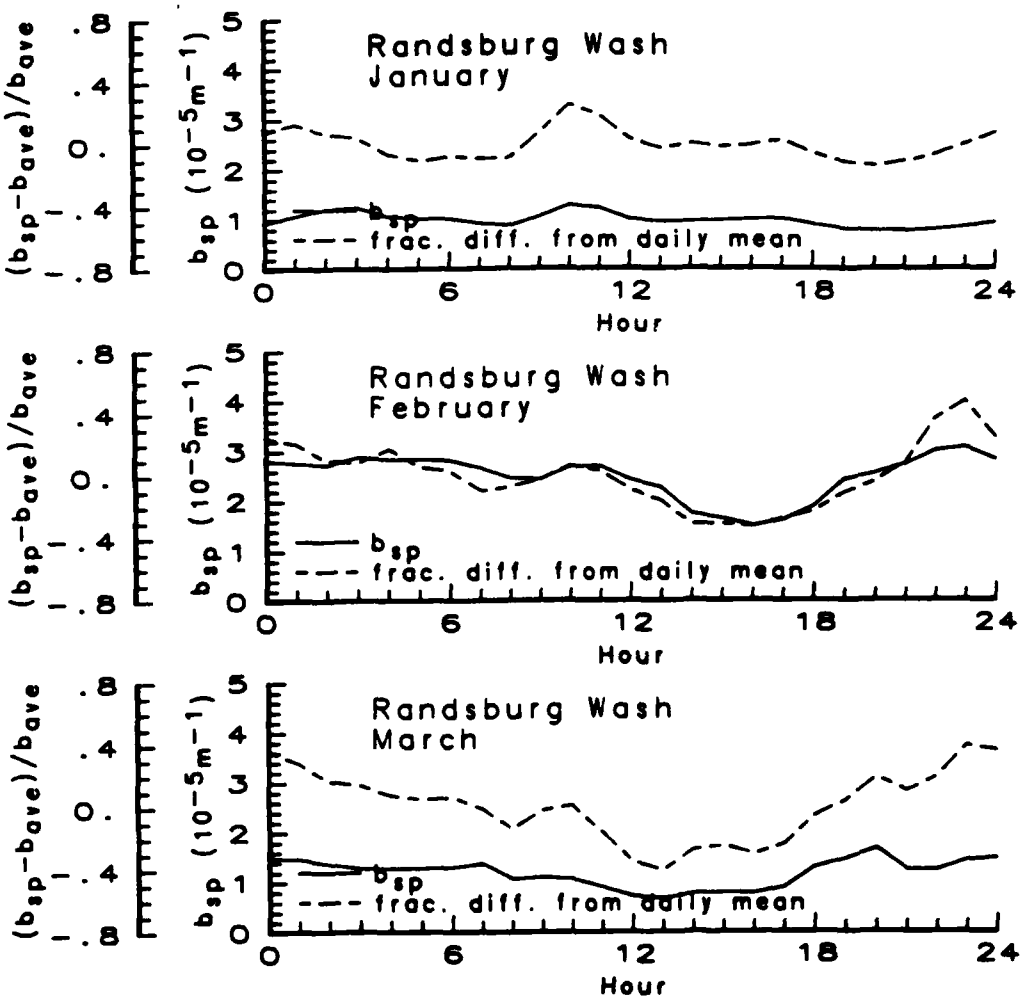

FIGURE A-4. Monthly Diurnal Patterns of Particle Scattering at Randsburg Wash.

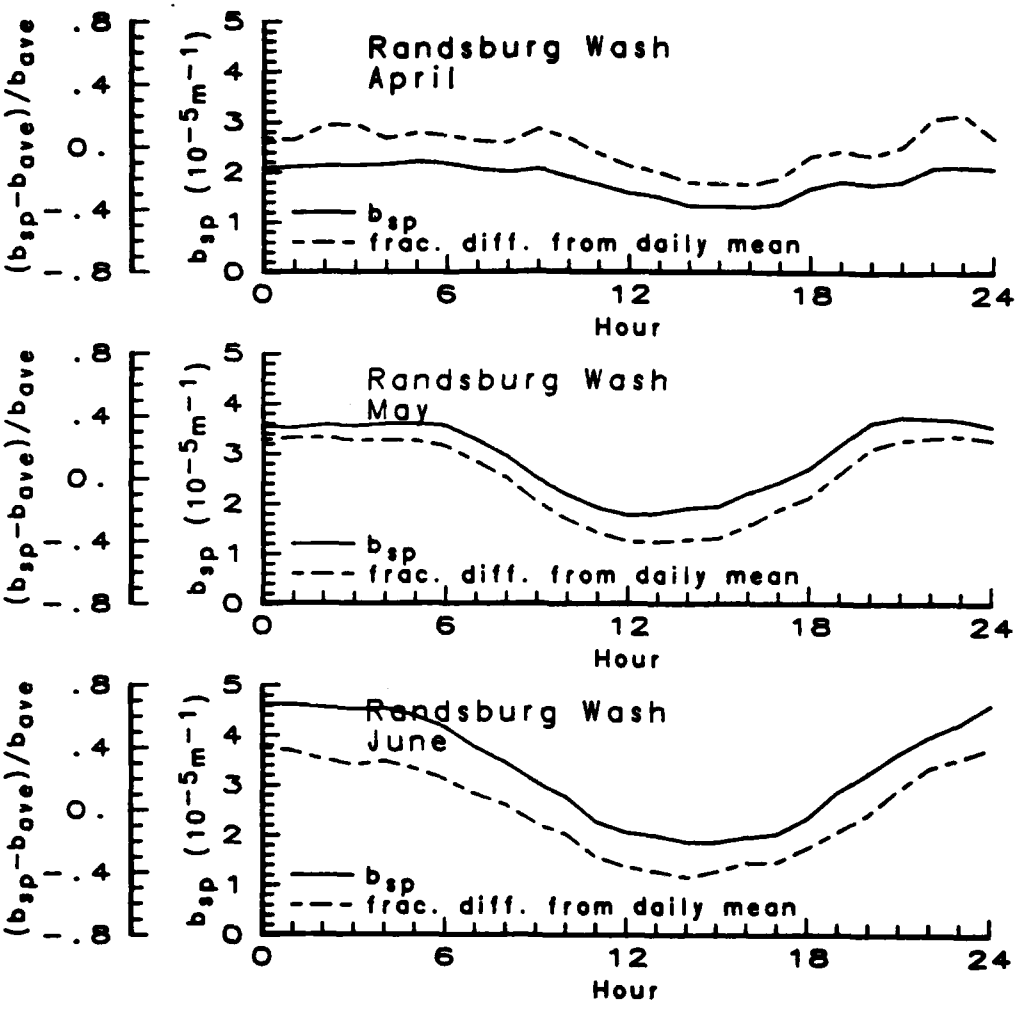

FIGURE A-4. (Contd.)

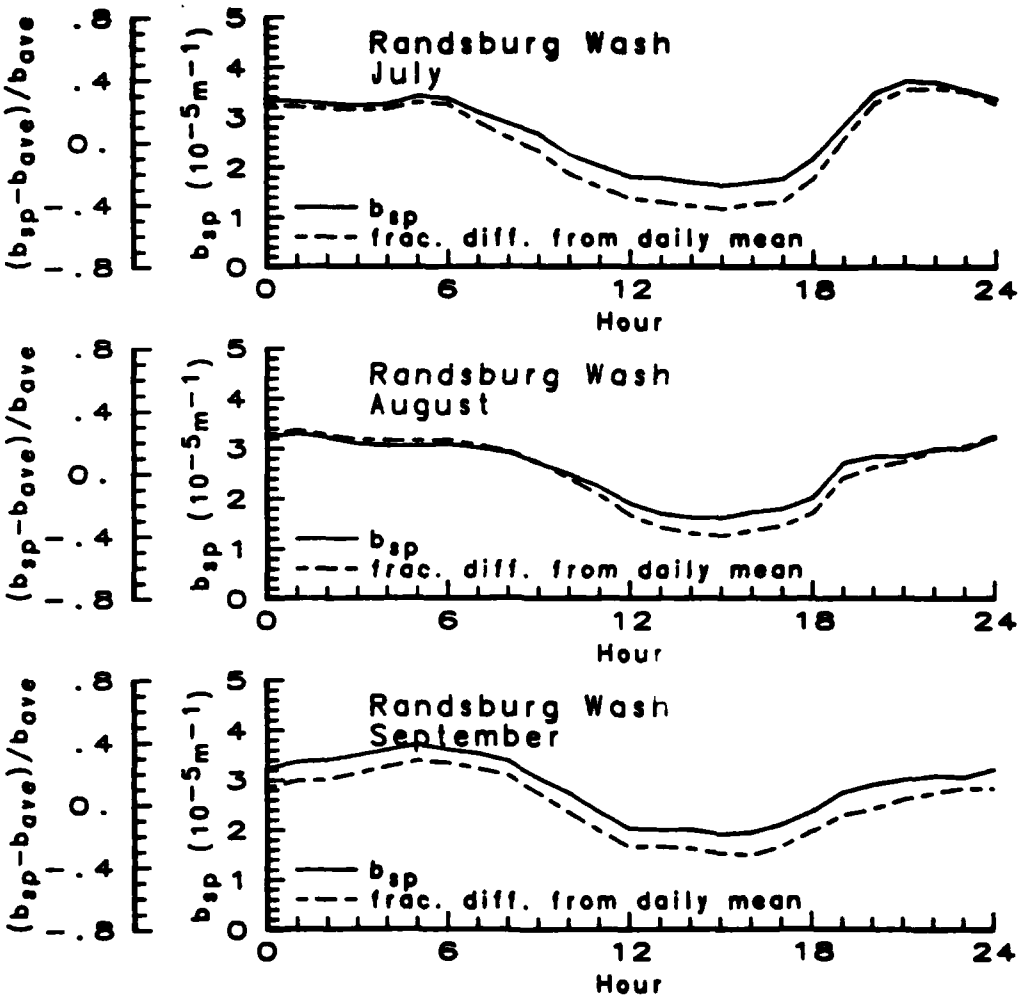

FIGURE A-4. (Contd.)

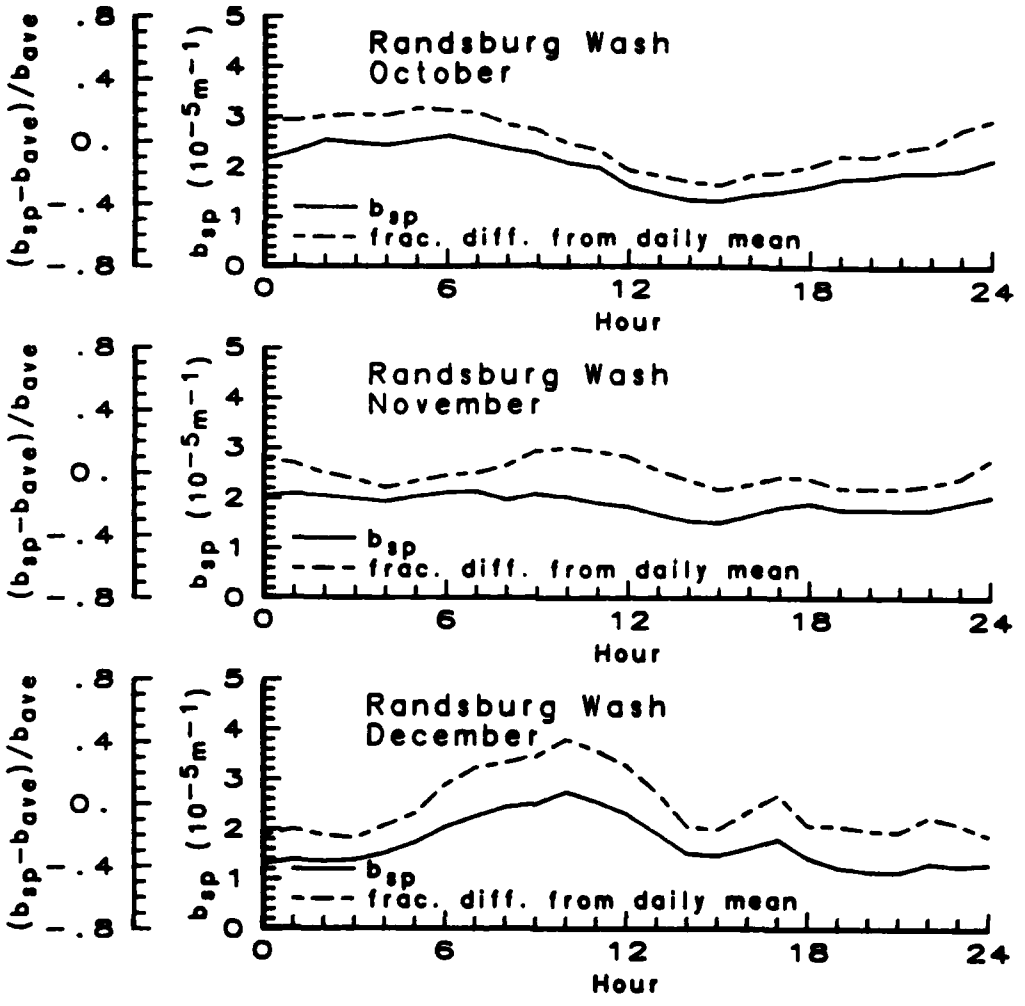

FIGURE A-4. (Contd.)

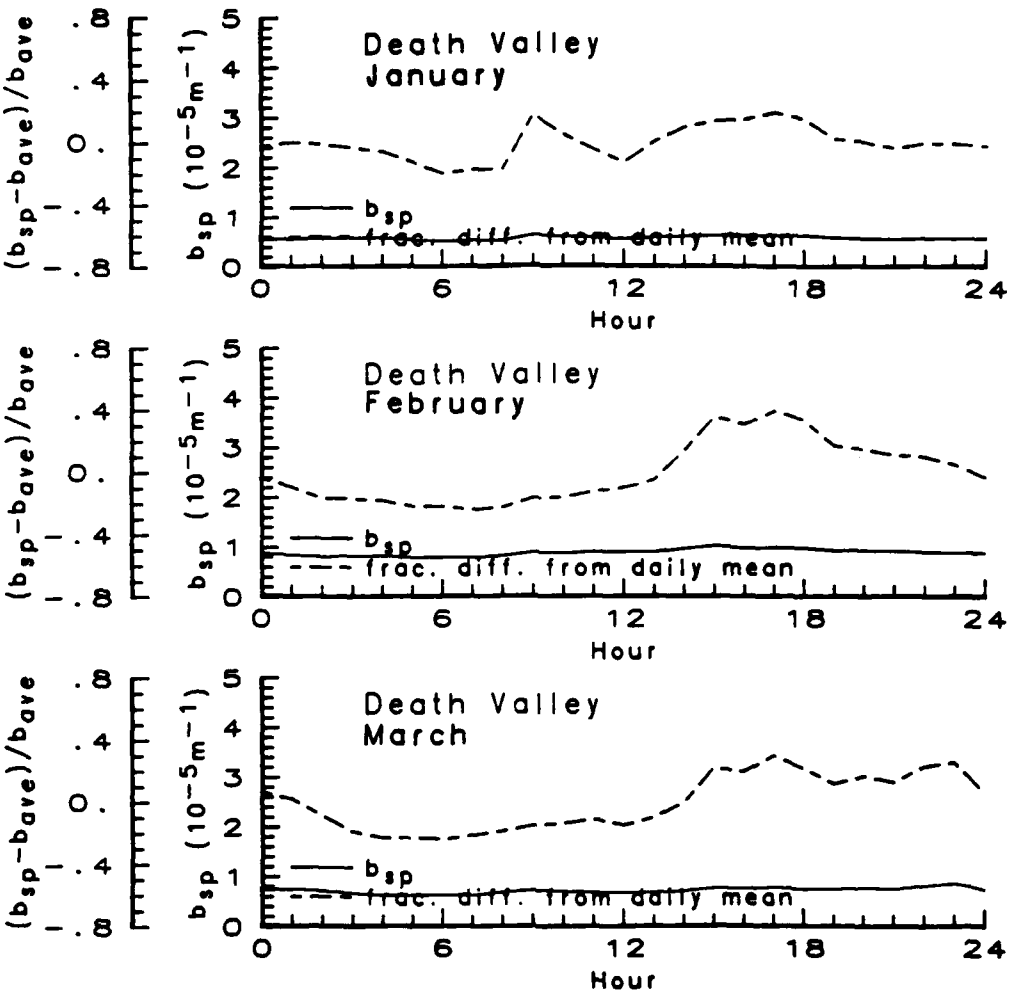

FIGURE A-5. Monthly Diurnal Patterns of Particle Scattering at Death Valley.

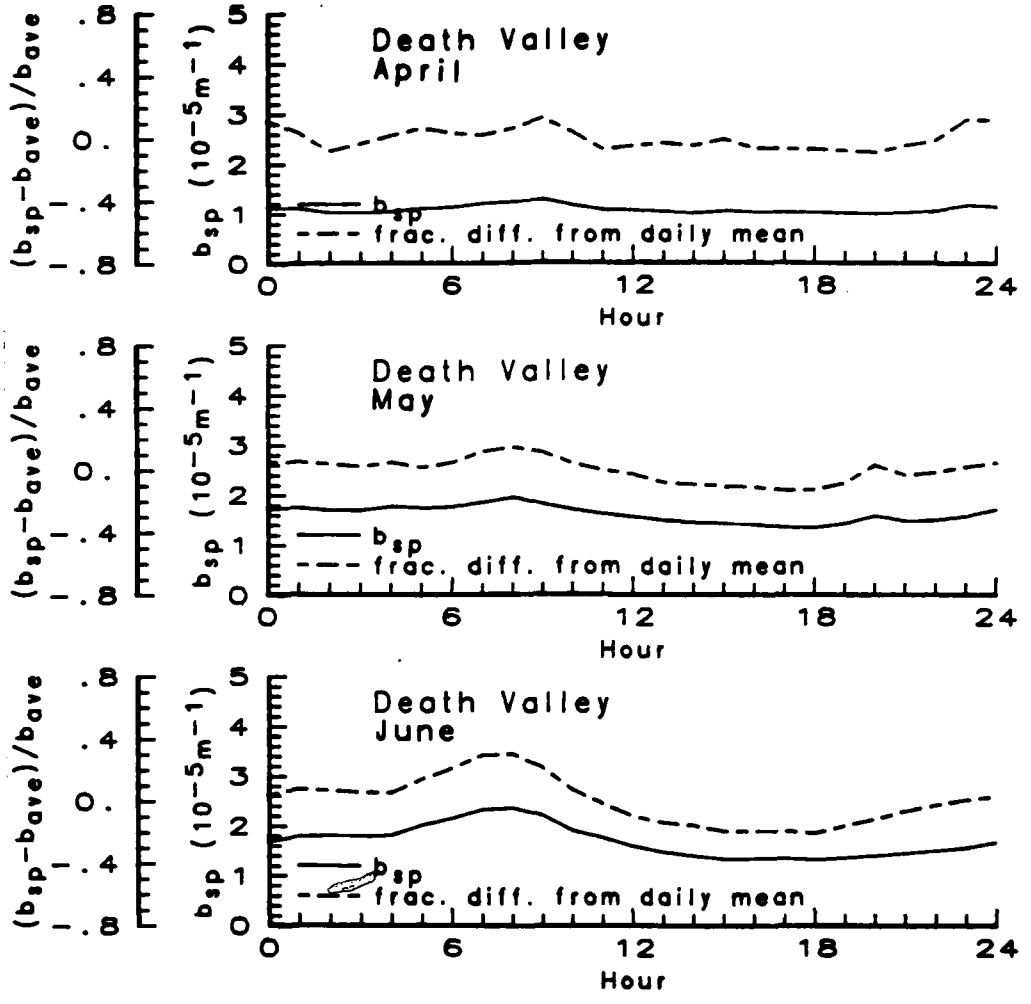

FIGURE A-5. (Contd.)

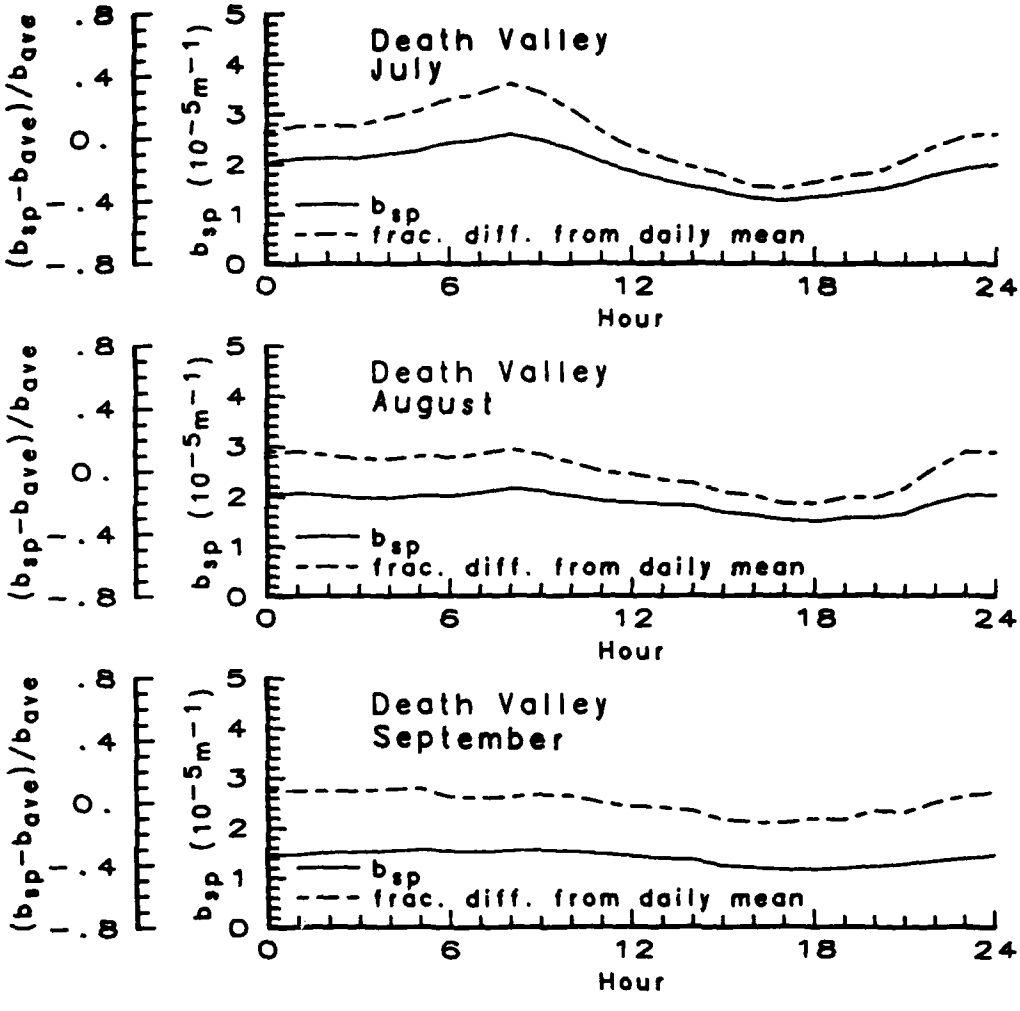

FIGURE A-5. (Contd.)

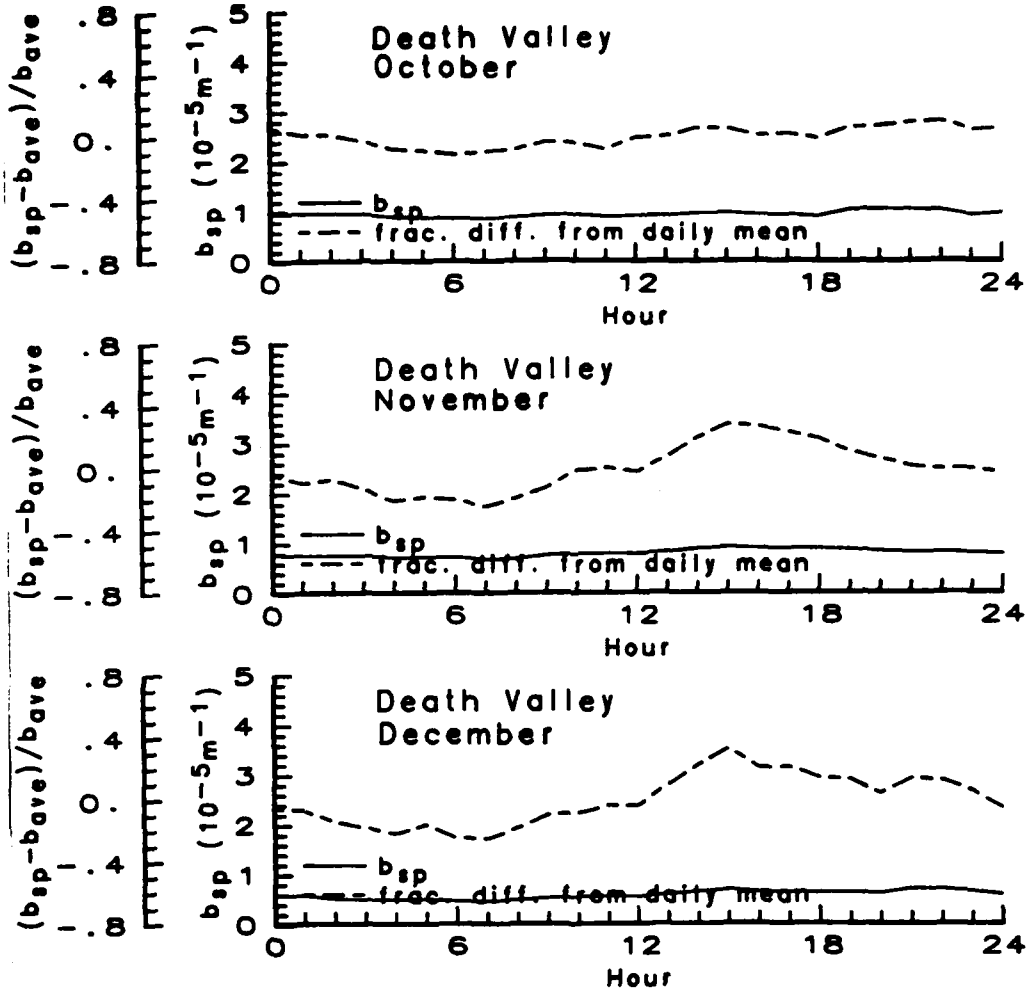

FIGURE A-5. (Contd.)

END

FILMED

11-84

DTIC